Rotor Blade Structure

Malo Rosemeier and Alexander Krimmer

Abstract The rotor blade is the key component of a wind turbine generator (WTG) and converts the energy of the wind into a mechanically useful form of energy. It represents a significant cost factor in the overall context of the turbine and at the same time has an enormous impact on the yield of the turbine. This chapter deals first with the normative requirements for the development and the verification of the serviceability and operational reliability of rotor blade structures. It then considers the loads acting on the rotor blade and the properties of the materials used. Furthermore, it addresses structural models for the analysis of blades and moreover discusses the design criteria for the topology and conventional manufacturing processes as well as deviations which occur. In addition, it considers the costs as part of the design process and their impact on the form of the blade structure, since the minimisation of the Levelised Cost of Energy is the main optimisation target when designing WTGs. Finally, it discusses blade materials from a sustainable development point of view. The chapter aims to provide a well-founded overview of a range of topics which are of relevance for the engineer working with the blade.

1 Introduction

The rotor blade is the key component of a wind turbine generator (WTG) and converts the energy of the wind into a mechanically useful form of energy. It represents a significant cost factor in the overall context of the turbine and at the same time has an enormous impact on the yield of the turbine.

M. Rosemeier (✉)
Fraunhofer Institute for Wind Energy Systems IWES, Bremerhaven, Germany
e-mail: malo.rosemeier@iwes.fraunhofer.de

A. Krimmer
TPI Composites Germany GmbH, Berlin, Germany
e-mail: a.krimmer@tpicomposites.com

A. P. Schaffarczyk (ed.), *Wind Power Technology*, Green Energy and Technology,
https://doi.org/10.1007/978-3-031-20332-9_5

Designing a rotor blade is a complex, iterative process which presents the design engineer with several challenges because of the overall structural concept of the rotor blade. For the development process to be successful, it is essential that the design engineer has sufficient understanding of the system, and hence the inclusion of the rotor blade chapter in this book is extraordinarily helpful. Starting from the system under consideration, it is possible to introduce simplifications which facilitate a mathematical-physical understanding and description of the problem, thus making the design problem amenable to a solution.

The main consideration in this chapter is the rotor blade structure for WTGs with horizontal axis (HAWT). This allows the rotor blade to be viewed as a cantilever beam which is fixed to the rotor hub via the blade bearing, also called pitch bearing. Here, it is subjected to aerodynamic loads on the one hand and to mass-induced loads, on the other. The second set of loads in particular means that strengthening the structure is generally accompanied by an increase in the mass and hence the load. Lightweight construction is thus necessary to counteract this so-called snowball effect.

To present a suitable approach to this problematic aspect, this chapter deals first with the normative requirements for the development and the verification of the serviceability and operational reliability of rotor blade structures. It then considers the loads acting on the rotor blade and the properties of the materials used. Furthermore, it addresses structural models for the analysis of rotor blades and moreover discusses the design criteria for the topology and conventional manufacturing processes as well as deviations which occur. In addition, it considers the costs as part of the design process and their impact on the form of the rotor blade structure, since the minimisation of the Levelised Cost of Energy (LCoE) is the main optimisation target when designing WTGs. Last but not least, it discusses rotor blade materials from a sustainable development point of view.

The chapter aims to provide a well-founded overview of a range of topics which are of relevance for the engineer working with the rotor blade. Those seeking more detailed information are referred to the literature referenced.

2 Normative Requirements

For construction approval, the release of the investment loan and the insurance of a WTG or a wind farm, the end customer/operator must have a type certificate. Section 2.1 begins by describing the route to the certificate for the key component, the rotor blade. Certification schemes relate to the standards and guidelines, which are based on a safety concept. Particular emphasis is placed on the Limit-State-Design concept, which is discussed in Sect. 2.2. Finally, an overview of the development cycle of a rotor blade is given in Sect. 2.3.

2.1 Certification

A type certificate confirms that a product (WTG) and its components (e.g. rotor blade or tower) have been assessed as being compliant with defined requirements regarding design and manufacture, for example. In Germany, the German accreditation body (DAkkS) qualifies accredited companies to issue these certificates in accordance with specific certification schemes, and technical standards and guidelines [64]. Examples of certification authorities, called IECRE Certification Bodies (RECBs) according to the IEC System for Certification to Standards Relating to Equipment for Use in Renewable Energy Applications (IECRE System), which hold an accreditation for schemes, standards and guidelines which are used for the certification of WTGs, especially for the rotor blade component [18], are: Det Norske Veritas (DNV) (operated separately until 2012 as DNV and Germanischer Lloyd (GL) and until 2021 combined as DNV GL), TÜV NORD, TÜV SÜD, TÜV RHEINLAND, DEWI- OCC as part of Underwriters Laboratories (UL) and BUREAU VERITAS.

The WTG manufacturer decides for one of the following certification schemes, each of which represents a consistent system of guidelines and technical standards, either according to the preference of the end customer or the economic aspects:

- GL 2010: "Guideline for the Certification of Wind Turbines" [42].
- DNVGL-SE-0441: "Type and component certification of wind turbines" [27] in conjunction with DNVGL-ST-0376 "Rotor blades for wind turbines" [26].
- IEC 61400-22: "Conformity testing and certification" [55] in conjunction with recognised standards and guidelines such as [26, 42, 60]. This scheme was replaced by IECRE System in 2018.
- IECRE OD-501: "IECRE System—Type and Component Certification Scheme" [57] in conjunction with OD-501-1 "Conformity assessment and certification of Blade by RECB" [58] and IEC 61400-5 "Wind energy generation systems—Part 5: Wind turbine blades" [60].

National requirements must also be fulfilled, if applicable. In Germany, for example, a WTG is deemed to be a building and must undergo type testing according to the guidelines of the German Center of Competence in Civil Engineering (DIBt) [24], see Chap. 7 of this book. This also includes an expert report for the rotor blade.

Depending on the scheme, the requirements for the design and manufacture of rotor blades are defined by one of the following standards and guidelines: GL 2010 [42], DNVGL-ST-0376 [26] or IEC 61400-5 [60]. What these fundamentally have in common is that they are based on the Limit-State-Design concept, see Sect. 2.2. The older GL 2010 differs from the latter two in the composition of the partial safety factors (PSFs), among other things. The latter two allow the PSFs to be reduced when detailed structural analyses or comprehensive validation tests on the full-scale blade test level of the testing pyramid (Fig. 1) or a level between coupon tests and full-scale blade tests are carried out.

Finally, a full-scale blade test is required for the component certificate of the rotor blade. This serves to validate the design assumptions on the one hand and to

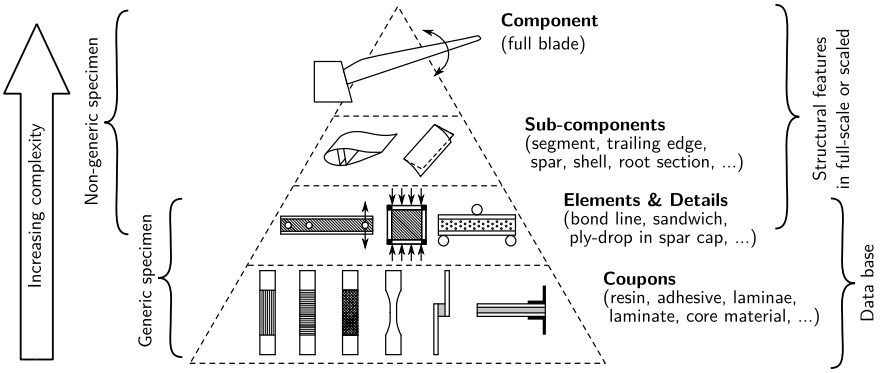

Fig. 1 Testing pyramid; based on [60]. Copyright © 2020 IEC Geneva, Switzerland. www.iec.ch

identify relevant failure modes or critical manufacturing details on the other [26]. In the full-scale blade test, the rotor blade is subjected to a testing program comprising static and cyclic tests, if applicable [56]. Test institutions which are accredited to test rotor blades in accordance with the IECRE System, so-called IECRE Test Laboratories (RETLs), include the following independent test institutes [61]: Fraunhofer Institute for Wind Energy Systems IWES, Blade Test Centre (BLæST), Offshore Renewable Energy (ORE) Catapult, Massachusetts Clean Energy Center WTTC and SGS.

2.2 Safety Concept

In engineering, three concepts exist to verify that a structure is safe against technical failure [92]: (i) the deterministic safety concept, also called Permissible Stress Design (PSD) or Allowable Stress Design (ASD), which is used in mechanical engineering; (ii) the semi-probabilistic safety concept widely used in construction engineering, also called Limit State Design (LSD) or Load and Resistance Factor Design (LRFD) and (iii) the probabilistic safety concept. In PSD, the resistance, i.e. the material limit value or the strength, is simply reduced by means of a global safety factor and compared to the internal load, i.e. the stress or strain present [143]. In LSD, in contrast, PSFs are applied to each action/load (external force or moment) or their effects and the resistance. An effect can be an existing load, deformation or stress resultant (internal force or moment), for example. A resistance can be a tolerable load, strength, deformation or stress resultant. The structural safety, also called failure probability, which is often expressed by the reliability index, plays a key role here. Probabilistic methods are frequently used to calibrate the PSFs to a target reliability index for a standard or guideline [63]. With LSD, it ultimately has to be shown that none of the crucial Limit State (LS) is exceeded in all relevant design situations [13].

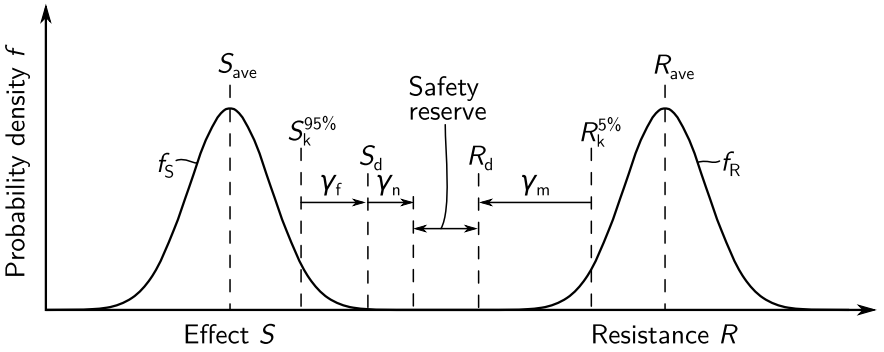

Fig. 2 Probability density functions of effect and resistance; based on [60]. Copyright © 2020 IEC Geneva, Switzerland. www.iec.ch

The standards and guidelines listed in Sect. 2.1 are based on the LSD. They state that for the rotor blade of a WTG in the ultimate limit states (ULS), the verifications must be provided for:

- strength failure,
- stability failure and
- fatigue failure.

In the serviceability limit states (SLS), the following must be provided:

- verification of the deformation limit.

For every limit state, a limit state equation can be formulated such that the resulting design value of the resistance R_d, for example a strength, is greater than or equal to the actual design value of the effect S_d, for example an existing stress, as a function of an action/load F_d [59]:

$$\gamma_n \cdot S_d\,(F_d) \leq R_d \tag{1}$$

Here, S and R are not quantities which can be measured directly, but variables which are subject to variance. Figure 2 shows the corresponding probability density function f_S and f_R about the average S_{ave} and R_{ave}. The characteristic values of the probable effect are therefore determined as a function of the characteristic action $S_k\,(F_k)$ as well as the expected resistance R_k of the rotor blade with the aid of methods based on probability theory, e.g. by considering the 95 % quantile of the effect and the 5 % quantile of the resistance. The corresponding design values R_d and S_d result from the application of PSFs to the characteristic values [23].

The PSF for the action/load γ_f, also called load factor [26], takes account of possible unfavourable deviations and uncertainties of the load as well as inaccuracies of the computational model [59]. Multiplying γ_f by the characteristic value of the action F_k gives the design value:

$$F_d = \gamma_f \cdot F_k. \tag{2}$$

The PSF for the resistance γ_m, also called the reduction factor [26], can take account of unfavourable deviations caused by adverse environmental conditions, temperature effects, manufacturing effects, the accuracy of calculation and validation methods as well as the resolution and combination of applied loads [60]. Dividing the characteristic resistance R_k by γ_m gives the design value:

$$R_d = \frac{R_k}{\gamma_m}. \tag{3}$$

Furthermore, a PSF γ_n is defined to take account of the severity of the consequences of a potential failure. Here, the components are classified into component classes 1–3, and different values for γ_n are specified for each of them [59]:

(1) Fail-safe structural components whose failure does not lead to a failure of another main WTG component and does not adversely affect the safety of the system as a whole. This requires a design with alternative load paths, so-called redundancy. Such a WTG component can be a replaceable main bearing, for example.
(2) Structural components with a safe life whose failure leads to the failure of another main component. The structure is designed such that no failure occurs during its service life. This means that the structures have a tendency to be heavier and must be replaced at the end of their service life. This WTG component class includes the rotor blade. The rotor blade may also be designed to be damage tolerant, however [60]. This concept allows damage to occur on components or structures that can be inspected well so that it is possible to notice the damage. The growth of cracks or damage is included in the calculation and the intention is for operation to continue from the point in time at which the damage occurs until the damage has reached a magnitude where it can be detected during an inspection. Critical growth of the crack which leads to a static fracture or excessive deformation, for example, does not happen during this phase between two inspections and the operational safety of the structure is maintained.
(3) Mechanical components with safe life which connect the actuators and brakes with main structural components for the purpose of non-redundant safety systems.

The safety reserve with respect to the target failure probability of the rotor blade in a limit state can then be expressed as the ratio of the design values, given by [25]:

$$\text{Safety Reserve Factor (SRF)} = \frac{R_d}{\gamma_n S_d}. \tag{4}$$

If the SRF ≥ 1, the verification was successful.

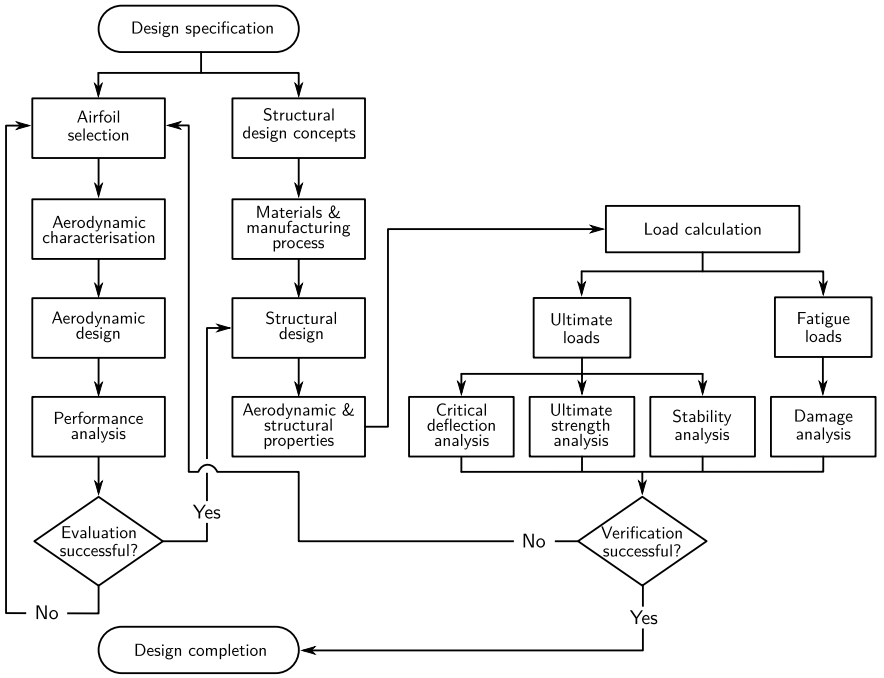

Fig. 3 Design process for WTG rotor blades; based on [60]. Copyright © 2020 IEC Geneva, Switzerland. www.iec.ch

2.3 Development Cycle of the Rotor Blade

The design process of a rotor blade from specification to completion is shown in Fig. 3. Fundamentally, two main development lines can be identified: (i) aerodynamic design and (ii) structural design. The two lines are conditional on each other and form a cycle, which is repeated several times. The objective is to optimise the rotor blade as the component and the WTG as the complete system so as to achieve maximum energy yield with minimum material usage and thereby realise the lowest possible LCoE. The mutual conditionality is discussed in detail in the sections below.

3 Loads

When a WTG is operating, different types of load act on its rotor blades and these are discussed in Sect. 3.1. Furthermore, the possible ways of calculating loads are illustrated in Sect. 3.2. Section 3.3 then goes on to describe the design load cases which are relevant for the verification. Finally, the effect of the dimensional scaling of blades is explained in Sect. 3.4.

3.1 Types of Load

The loads on a rotor blade of a WTG are subdivided into external and internal actions. The external actions/loads include the gravitational load, the aerodynamic loads induced by the wind and the rotation, and the inertial loads generated by the rotational acceleration and rotation. The internal actions/loads include residual stresses caused by a change in temperature.

Figure 4a depicts a schematic of the wind field acting on the WTG. This wind field can be split up into a deterministic component, which is generated by wind shear and is described as a function of the height $v\,(h)$, and a stochastic component $v\,(t)$, which arises as a result of (i) the turbulence as a consequence of the ground unevenness at the site and also the wake of other WTGs in a wind farm situation, which is characterised by the effective turbulence intensity [59]; (ii) changes in wind direction or (iii) gusts, see Chap. 3 of this book. It becomes clear that the rotor blade is exposed to a different wind load situation depending on the azimuth angle position of the rotor.

The gravitational force F_g acts on the centre of mass, which is at around 1/3 of the blade length (Fig. 4b), and causes an alternating bending moment in the sweep direction (lead-lag) M_x (Fig. 4d) as a consequence of the rotation.

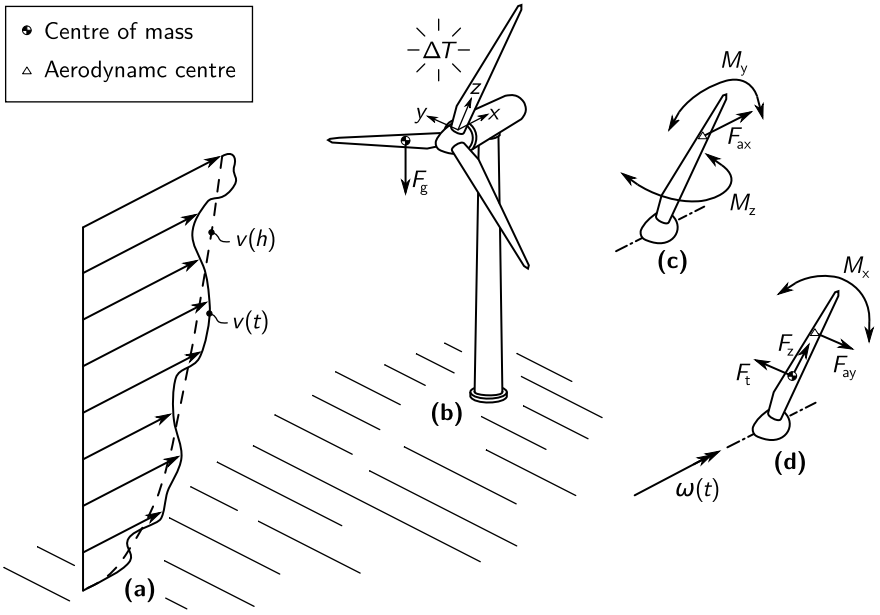

Fig. 4 Loads acting on the rotor blade: wind field (**a**), gravitational load and temperature change (**b**), aerodynamic load component, flapwise bending moment and twisting moment (**c**), aerodynamic load component and inertial force and lead-lag bending moment and rotor acceleration as well as centrifugal force (**d**); based on [103].

In the speed-controlled partial load regime, the aerodynamic load acts on the aerodynamic centre, which is at around 2/3 of the blade length. It is generated by lift and drag on the airfoil (see Fig. 11 in Chap. 4 of this book), which can be split up into a drive component in the sweep direction F_{ay} (Fig. 4c) and a thrust component in the flap direction F_{ax} (Fig. 4d). These force components then correspondingly cause a lead-lag bending moment M_x and a flapwise bending moment M_y (Fig. 4c). In the full load regime, the power of the WTG is controlled with the blade pitch angle, which reduces the aerodynamic load. If the blade pitch angles of the three rotor blades are not synchronised with each other, for example, because they are installed incorrectly, this situation leads to an aerodynamic imbalance, whose impact for the non-rotating components, such as the tower, can be crucial [112]. Conventional practice is to mount the rotor blades in a cone angle with respect to the rotor plane to increase the tower clearance. When the blade is thought of as a rigid body, the aerodynamic load would generate a twisting moment M_z (Fig. 4c) at the blade root because of the cone angle and also because of the geometric flapwise pre-bend of the blade. In reality, however, the blade is flexible so that, especially in rated operation, the aerodynamic load component F_{ax} bends the blade back into the direction of the rotor plane, which in turn reduces the twisting moment M_z at the blade root. A pre-bend of the blade in the sweep direction, particularly in the direction of the blade trailing edge, has a similar effect. Here, the aerodynamic load generates a twisting moment M_z, which twists the blade at the tip and thus leads to a locally smaller blade pitch angle, which in turn reduces the aerodynamic load and thus the bending moment at the blade root [9]. Aerodynamic instabilities such as flutter can occur in an overspeed situation, in which aerodynamic forces couple the torsional resonance mode with a flapping resonance mode [47]. The flutter resonance thereby produced results in a twisting moment M_z and a flapwise bending moment M_y.

Inertial forces F_t (Fig. 4d) arise when the rotor is accelerated or decelerated ($\omega(t)$), and result in a lead-lag bending moment M_x. In the idling or stationary situation with lateral inflow, the rotor blade can be excited in its resonance mode in the sweep direction when the excitation frequency resulting from vortex-induced lateral vibrations and the resonance frequency of the blade couple in resonance [51]. The vibration generates an inertial force F_t which acts on the centre of mass and then causes a lead-lag bending moment M_x.

Furthermore, the rotation generates a centrifugal force F_z in the rotor plane (Fig. 4d). This can induce an aerodynamic and mass imbalance when the blade masses are not balanced, as can occur as a result of ice accretion, for example. With the rigid blade, the cone angle would cause a portion of F_z to produce a bending moment in the flap direction M_y. As described above, this is reduced again by the actual flexibility of the blade in rated operation. The centrifugal force has a stiffening effect with increasing rotor speed and thus has an impact on the blade resonance frequencies [39].

A temperature change to the blade structure produces intrinsic mechanical loads. These build up during the cooling process of the rotor blade after the materials have cured because the materials have very different thermal expansion coefficients.

Depending on the operating temperature of the WTG, significant residual stresses can be generated, for example in the adhesive joints [108].

3.2 Load Calculation

For the aero-servo-elastic simulation of the loads, the aerodynamics are modelled with the aid of Blade Element Momentum Theory (BEM), Vortex Methods or Computational Fluid Dynamics (CFD). They are coupled to the WTG structure, which is either discretised by spring-mass damper systems, finite element (FE) systems or modally modified beams. The WTG states are adjusted by a speed and blade pitch angle controller. The structural model of the WTG is thereby subjected to so-called Design Load Cases (DLCs). These not only consider situations which occur in operation, but also extreme situations such as gusts, emergency stops and grid loss [59]. Commonly used simulation environments for the time as well as for the frequency domain include HAWC2/HAWCStab2 [20], OpenFAST [87], Bladed [22], MoWiT [36], Adams/AdWiMo [84], Flex [90], ADCoS [1], Cp-Lambda [95], alaska/Wind [62] and Simpack [21]. A comparison of different simulation environments can be found in [66, 96], for example.

In particular, the mass-load-induced fatigue load spectrum as the crucial load in the blade root region can already be estimated with little simulation effort [110]. To this end, the number of rotations during the total life and the static mass moment, which results from the product of the total mass and the lever arm between blade root and centre of mass (Fig. 4b), is considered.

3.3 Design Load Cases

The mechanical loads from the simulations are summarised in the design load cases for the rotor blade, which are explained below. These design loads can be specified either for an individual type of WTG or as a broad design load envelope for several versions of a WTG type [59].

3.3.1 Load Case of Minimum Tower Clearance

For this load case, the simulation time series are examined for the minimum distance between tower surface and blade tip. The load state along the blade, particularly flapwise, dimensions the maximum permissible blade tip deflection.

3.3.2 Extreme Load Envelope

This load case involves a load envelope, and means that the simulation time series are examined for their maximum and minimum values for every cross section along the rotor blade. In general, the load vector components of an envelope do not occur at one and the same time. The extreme loads, which are extracted as point clouds, are therefore enveloped and projected into the four main directions, for example, and also in more than four sectors. At least 12 sectors are required for the blade root, for example, [60]. A projection method is illustrated in [26].

3.3.3 Fatigue Load Spectra

For this load case, the simulation time series are processed with the aid of load cycle counting methods, for example, Rainflow Counting [77], see Fig. 4 in Chap. 7 of this book. This results in load spectra, also called Markov matrices or range-mean matrices. A collective consists of a number of cycles n_i, a mean stress $S_{\mathrm{m}i}$ and a stress amplitude $S_{\mathrm{a}i}$. The usual procedure is to add the total damage of all collectives together using the linear damage accumulation hypothesis according to Palmgren [91] and Miner [82]. The use of load spectra for the structural analysis can become relatively computationally intensive when high sectoral resolution is desired. For this reason, load spectra of force or moment time series are also used, and then Damage Equivalent Loads (DELs) for a reference number of cycles to failure n_{ref} and a material-specific negative inverse exponent of the fatigue life curve m [52] are derived therefrom, see Fig. 5 in Chap. 7 of this book. One disadvantage of using DELs is that it is almost impossible to take the influence of the cycle means into account. This appears to be critical since the matrix materials of fibre-reinforced polymer (FRP), in particular, are extremely sensitive to mean stress [122]. However, when the DELs have high sectoral resolution within a blade cross section, it does seem possible to take mean stress effects into account nevertheless [97].

3.3.4 Loads from Changes in Temperature

This load case results from the boundary conditions of the rotor blade manufacturing process. In the simplest case, the temperature difference ΔT between curing and operating temperature can be used here, cf. [3, 108, 109]. Internal loads caused by stresses from temperature changes and the different thermal expansion coefficients of the individual materials can be added to the extreme loads and taken into account in the fatigue load spectra as a static average [74].

3.4 *Effects of Scaling*

GALILEO's square-cube law [38] applies to the scaling of WTG rotor blades as it does to all other three-dimensional (3D) bodies, and is referred to below as the scaling law. It states that for the linear scaling of a body, its surface area increases as the square of its length and its volume increases as the cube of its length. Consider a cube with edge length L_1 as shown in Fig. 5. If the cube is scaled such that the edge length doubles to L_2, then the base area A_1 in the figure scales by a factor 4 to the base area of the scaled cube A_2. In this process, the volume of V_1 increases by a factor of eight to the value V_2. This means that when the length of the rotor blade is doubled, its mass increases eightfold according to the scaling law.

A selection of different structural concepts for rotor blades is plotted in Fig. 6 and shows rotor blade mass as a function of the rotor diameter. The selection includes all wind classes, material combinations and generations of the last 30 or so years. The regression took account of all blades made from glass fibre (GF) in epoxy resin (EP) and this results in an exponent of approx. 2.2. When the regression is carried out separately for different structural concepts for rotor blades, the exponents lie between 1.9 and 2.8 [72]. Hence, the structural masses of rotor blades do not in fact increase proportional to the third power, as expected according to the scaling law, but roughly proportional to the 2.4th power of the rotor blade length.

The reason for the exponent in the scaling must be sought in the type of loading of the rotor blade. As has been described above, rotor blades are mainly exposed to two types of loads: gravitational loads from their own mass on the one hand and loads from the aerodynamic action on the other.

The mass loads of a rotor blade depend directly on its mass and thus its volume, while the aerodynamic loads are determined by the aerodynamic surface of the blade. Like the surface area of the rotor blade and thus the aerodynamic loads, the cross-sectional areas of the rotor blade increase as the square of its length. These cross-sectional areas form the resistances against the loads. This means the aerodynamic loads do not lead to a disproportionate increase in mass. As shown, the volume and therefore the mass loads increase as the third power of the length, however, which means that the cross-sectional areas have to increase disproportionately. This explains first of all why the mass of the rotor blade structure which has to withstand these loads increases by a value which lies between the two powers 2 and 3, i.e. around 2.4.

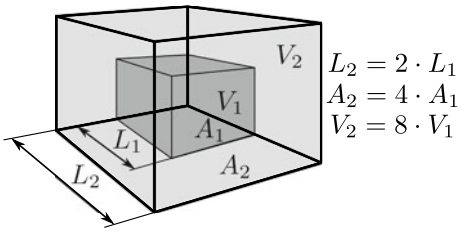

Fig. 5 Scaling using the example of a cube; based on [73]. Copyright © 2017 Alexander Krimmer

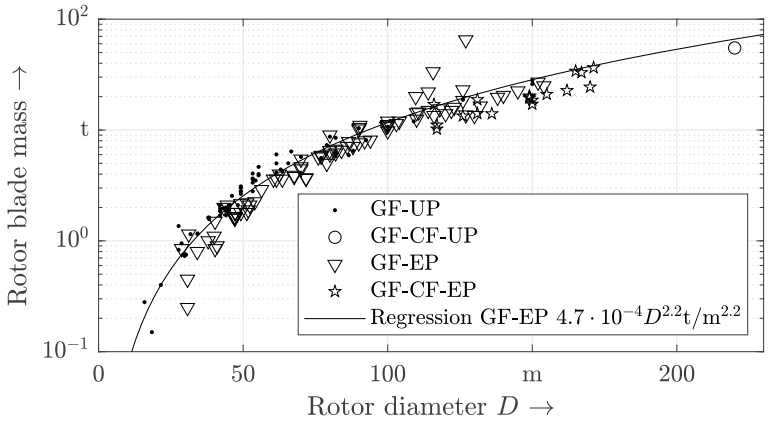

Fig. 6 Masses of various structural concepts for rotor blades: Glass fibre (GF)-reinforced unsaturated polyester resin (UP) (GF-UP); GF-reinforced skin laminate and carbon fibre (CF)-reinforced spar cap with unsaturated polyester resin (UP) (GF-CF-UP); GF-reinforced epoxy resin (EP) (GF-EP); GF-reinforced epoxy resin (EP) (GF-EP); GF-reinforced skin laminate and CF-reinforced spar cap with epoxy resin (EP) (GF-CF-EP); based on [72].

Furthermore, the aerodynamic loads of a rotor blade in the lee direction, the downwind direction, cause a more quasi-static deformation, while the rotation of the rotor leads to a cyclically changing bending load of the rotor blade with each revolution resulting from its own mass. It thus becomes clear that it is primarily the service loads which increase disproportionally when scaling rotor blades and greater consideration will have to be given to these loads in the future.

4 Materials

The rotor blades of WTGs are composed of a large number of different materials. The main components are fibre-reinforced polymer (FRP), whose composition, properties and processing are discussed in Sect. 4.1. Core materials are also used to guarantee stability in the thin-walled rotor blade structures, and their properties and modes of action are presented in Sect. 4.5. Furthermore, rotor blades usually contain structural adhesives, whose properties and tasks are documented in Sect. 4.6. A frequently underestimated task concerns the coating materials, which can be found in Sect. 4.7. Moreover, various metals are used in the lightning protection system, at the blade connection and at a segmented-blade joint. They are presented in Sect. 4.8.

4.1 Fibre-Reinforced Polymers

FRPs have largely become established as the main structural material in the manufacture of rotor blades. Blades manufactured nowadays consist primarily of glass fibres (GFs) in an epoxy resin (EP) matrix. A smaller number are likewise constructed from GF, but embedded in unsaturated polyester resin (UP). Furthermore, there is an increasing tendency to strengthen the main reinforcing elements of rotor blades with carbon fibres (CFs). For the main spar caps, the use of pultruded unidirectional (UD) plates has become established. These are also manufactured with CFs in various resin matrices such as EP, UP and vinylester (VE).

There are a variety of reasons for using FRPs, the most important ones being:

- high strength,
- high stiffness,
- low density,
- advantageous fatigue strength properties,
- ease of manufacture and
- simple production of the components in freeform surfaces.

Figure 7 shows the structural principle of FRPs with their important components. The laminate (Fig. 7a) is composed of laminae or plies, as they are shown in Fig. 7b with information on the fibre orientation, for example, when one of the plies is a UD fibre-reinforced single ply. Furthermore, core materials in a sandwich laminate or adhesive layers between two substrate laminates, which are the bonded elements, can also be considered as single ply. The fibre-reinforced UD single ply, as shown in Fig. 7c, is composed of

- fibre,
- sizing and
- resin matrix.

The fibre itself, as illustrated in Fig. 7d, is usually surface coated with sizing, which bonds chemically with the resin matrix.

The question is why fibres in particular have such excellent mechanical properties. The observations by GRIFFITH [44] are the simplest way to explain this. Figure 8 shows the results of his experiments. It is clearly evident that the strength of the GF considered increases disproportionally when their diameter is decreased. This is because the probability of damage becomes lower with decreasing fibre cross section, an effect which is known as the fibre paradox.

To make these properties available for use in structural mechanics, the fibres are embedded in a so-called matrix. In the case of rotor blades, this nowadays consists of polymers such as EP and UP, but researchers are also experimenting with polyurethane (PU) and polymers with thermoplastic properties [85] as well. The task of the matrix is to transfer the forces acting on the structure into the fibres. These forces are primarily transferred via shear. Furthermore, the matrix provides the dimensional stability of the basic textile framework and guarantees that the fibres are protected from external influences.

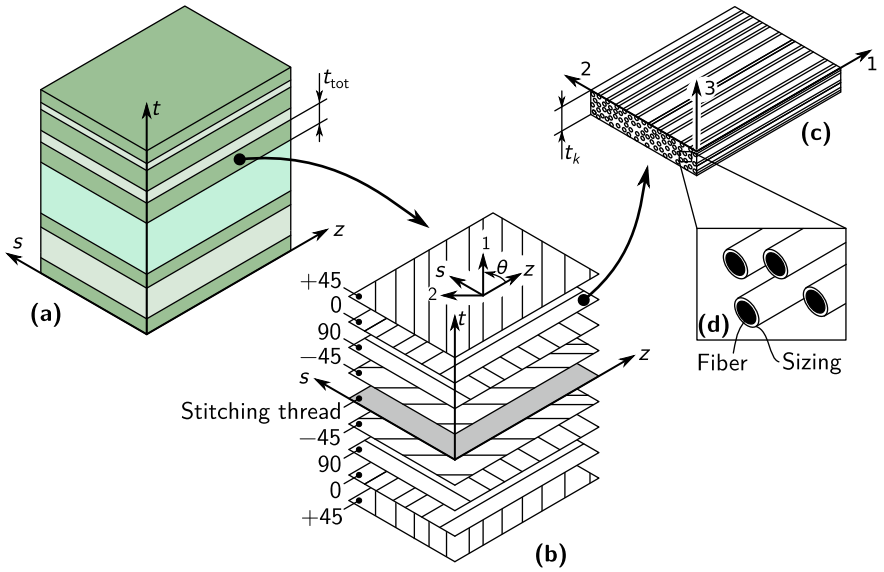

Fig. 7 Layup stacking with various laminates (**a**); fibre-reinforced polymer (FRP) laminate (**b**); lamina (**c**); fibre and sizing (**d**); based on [111]. Copyright © 2020 Malo Rosemeier

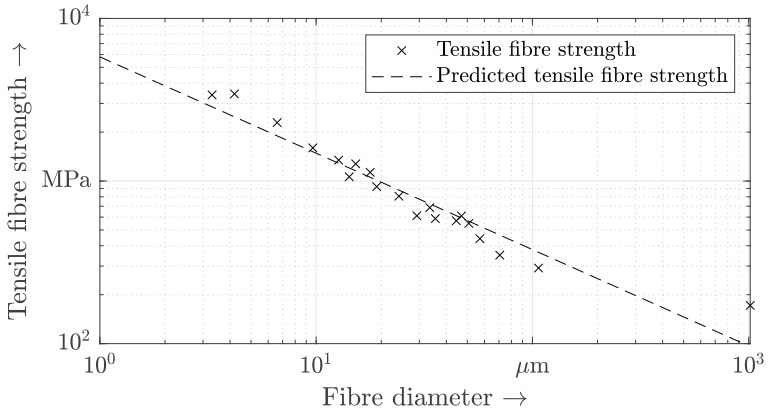

Fig. 8 Tensile strength of glass fibre (GF); data from [44]. Copyright © 2021 Alexander Krimmer

Table 1 Conventional mechanical properties of materials

Property	E-glass	HT carbon	EP matrix
Young's modulus longitudinal/transverse in GPa	80	240/15	3.00
Shear modulus transverse/longitudinal in GPa	32	45	1.07
Poisson's ratio transverse-longitudinal	0.25	0.3	0.4
Tensile strength in MPa	2000	4000	70
Strain at fracture linearised in %	2.5	1.67	2.3
Negative inverse stress-life curve exponent	10	14	10
Density in kg/m^3	2600	1800	1150
Coefficient of thermal expansion long./trans. in 10^{-6}/K	5.3	-0.6/20	60
Price in €/kg (in 2021)	1.00	15.00	4.00

The most important mechanical properties for the most important materials which form the FRP are given in Table 1. The properties for orthotropic high-tenacity (HT) CF are stated in the fibre direction (longitudinal) as well as orthogonal to it. The mass-related prices given must be understood as rounded guide values, while the actual prices are naturally subject to market fluctuations.

Other materials such as R-GFs are also suitable for use in rotor blades. They have a modulus of elasticity (Young's modulus) which is 10 % higher than that of E-GFs. Since only an introduction to the topic is provided here, the selection is limited to the materials most frequently used.

4.2 Semi-Finished Textile Products

The FRP used in the rotor blade structures is usually non-crimped fabrics (NCFs) in the form of semi-finished textile products. These fabrics are characterised by the fact that several fibre plies in the form of GF rovings are laid one on top of the other with different orientations by machine before being stitched together. This increases the number of raw materials involved by the stitching thread, which usually consists of polyethersulfon (PES). A tri-axial (TX) NCF is depicted in Fig. 9.

Woven fabrics can also be used for the manufacture, for example. Their disadvantage is that the waviness or undulation of the fibres is greater because the plies are interwoven, and it is thus not possible to exploit the mechanical properties of the fibres to the same extent. Further details can be found in [116].

The text below is therefore based on NCFs for the manufacture of WTG rotor blades. A so-called non-crimped fabric composite (NCFC) is thus produced in the manufacturing process, which then requires that different NCFs have to be characterised in the composite. The types of NCFs usually used in rotor blades are UD, bi-axial (BX) and TX NCFs.

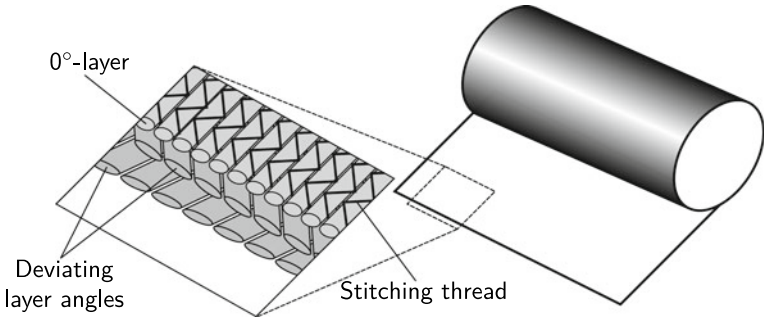

Fig. 9 Schematic diagram of tri-axial non-crimped fabric [72]. Copyright © 2014 Alexander Krimmer

4.3 Materials Testing

To now make rotor blade structures predictable, the mechanical properties of the materials and of the FRP in particular must be known. These can be determined by means of materials testing on the coupon level of the testing pyramid (Fig. 1). Corresponding normative stipulations for this are given in [60]. Materials testing can be carried out at different levels of the testing pyramid involving different amounts of effort and with varying levels of validity. The main challenge consists in the fact that the properties of the rotor blade materials evolve only during the manufacturing process of the rotor blade structure. They are affected significantly by the process parameters during rotor blade manufacture and also by the properties of the semi-finished fibre material and the matrix. The most important ones are

- manufacturing methods (hand layup (HL), vacuum infusion (VI) or others);
- accuracy during layup of the material;
- process pressure;
- consequential compaction and fibre volume fraction (FVF) and
- temperature profile during processing and curing.

To be able to determine the properties accordingly, these process parameters have also to be set as best as possible during the production of the material samples. This naturally means that the same semi-finished products and resins as in the rotor blade must be used for the testing.

Since FRPs are orthotropic materials, i.e. materials with anisotropic properties, at least three tests must be carried out on each semi-finished product to characterise the elastic properties. These are tensile tests in the main reinforcement direction and at right angles to it, as well as a test to determine the shear properties. It is thus possible to determine the required tensile and shear strengths. If it is additionally desired to determine the required compressive strengths as well, then compression tests in the main reinforcement direction and at right angles to it are also required.

More tests or fewer tests have to be carried out on the different NCFs used depending on the complexity of the material model used. Materials testing is usually associated with high costs, which have to be kept low. An effective way of keeping the number of tests as small as possible is to use Extended Inverse Laminate Theory (EILT) [72]. This allows a generic material model to be parametrised right down to the elastic and strength properties of fibre and matrix.

4.4 Elasticities of the Unidirectional Single Ply

EILT is based on the inverse execution of classical laminated plate theory (CLPT) [101, 135]. It is an established and effective tool for predicting the properties of layered FRPs.

To carry out CLPT, all that is required is the two-dimensional (2D) compliance matrix which describes the planar stress state. If the intention is also to determine the elastic properties of a laminate expressed in three dimensions (3D), then it is necessary to already establish the properties of the single ply in 3D. Inverting the matrices leads in each case to the elasticity matrices of the single ply. For the 2D case, all further steps are described in [101, 135]. For the 3D expression of the laminate properties, reference is made to the work of CHOU [16]. He formulates a suitable method to calculate them.

Starting from the expression of the compliances and stiffnesses of the individual ply, an inverse calculation right down to the properties of the individual components, fibre and matrix, is performed using micromechanical rules of mixture as part of EILT. If these properties are known, the micromechanical rule of mixtures can again be used to predict the properties of UD single plies.

Software is available from different institutions and with different capabilities which can rapidly and simply generate predictions for mechanical properties of FRPs. Mention is made here of two of them, which are available for free and provide a simple introduction to the topic.

AlfaLam Advanced Layerwise Failure Analysis of Laminates (AlfaLam) is a program based on CLPT which is made available by the Leichtbau und Bauweisen (KLuB) Institute at the TU Darmstadt. It can be found on the KluB download page [125]. The program versions deposited there date from 2009, however.

eLamX^2 is likewise based on CLPT and is made available by the Institute of Aerospace Engineering at the TU Dresden [50]. eLamX^2 likewise provides a user forum and is regularly updated. Moreover, an impressive overview of the capabilities and possibilities of the software is provided at [50].

eLamX^2 also includes micromechanical rules of mixture, but their forecasting accuracy is limited. To achieve better results, attention is drawn to HASHIN and ROSEN [49], whose procedure is likewise used in [135] as well as the micromechanical equations in [74]. The latter were used to provide an overview of the mechanical behaviour of a GF-EP-UD single ply as a function of the FVF in Fig. 10.

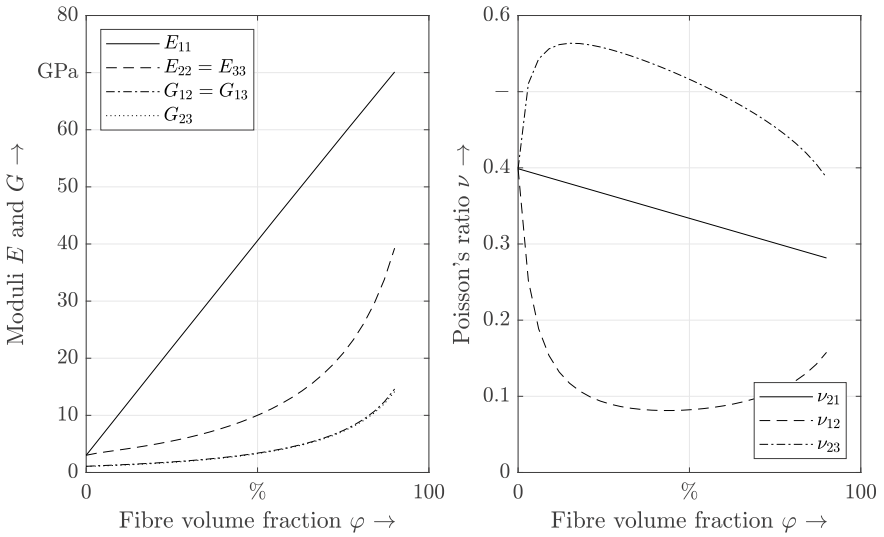

Fig. 10 Mechanical properties of a glass fibre-epoxy resin unidirectional (GF-EP-UD) single ply.

If a more detailed examination of the topic of FRPs is to be conducted, it is recommended that you program the CLPT yourself in accordance with [101, 135], for example. A good introduction is provided by the Python implementation compmech [12].

4.5 Core Materials

Rotor blades for WTGs are thin-walled structures in the best sense of the word. Such structures are usually prone to buckling, which is a stability failure phenomenon of planar load-bearing structures. Under in-plane compressive loading, the load-bearing structures give way from the load direction and consequently do not absorb additional forces [141]. In the rotor blade, this applies to the skin laminate sections of the rotor blade structure. They are the easily recognisable sandwich sections in Fig. 16.

To prevent this stability failure, the skin sections of the rotor blade are built as sandwich structures. In the rotor blade, they consist of the outer and inner skin laminates or skins, which are kept apart by a core to increase the parallel-axis component of the area moment of inertia and thus the bending stiffness of the sandwich cross section. This core is usually flexible and has comparatively high shearing rigidity. In order not to significantly increase the structural mass of the rotor blade at the same time, materials are used which comply with this requirement and have a low density. In the rotor blade, these are predominantly:

- polyvinyl chloride (PVC) foam,
- polyethylene terephthalate (PET) foam,
- PU foam and
- end-grain Balsa wood.

The core materials are usually supplied as sheets. If they are orthotropic materials, as is the case with PET foam and end-grain Balsa wood, the directions of the highest elastic modulus are oriented in the thickness direction of the plates. This explains why end-grain Balsa wood is used, for example, which is characterised by the fact that its direction of growth points into the thickness direction of the plate.

The core materials mentioned here are not flexible enough to follow the contours when they are laid into the rotor blade mould, however. Therefore, if a curvature has to be introduced into the core material plates, a fabric is bonded on one side and slots are made in the other side of the plate with a saw or a knife. This process allows the plates to be draped along the contours. Furthermore, the plates are partially perforated to ensure that the resin flows through the thickness of the plate. A perforated and slotted PVC foam plate is depicted in Fig. 11a.

The fact that resin of very low viscosity is used in the VI process has a disadvantageous effect. It fills the cavities which are present in the dry stack-up, and thus the perforations and slots described above are filled with resin, for example. Furthermore, open cells at the surface of the core material fill as well. The resulting resin intake of the core is described in [88, 107] and made amenable to a calculation. This is absolutely essential for a reliable prediction of the mass for the rotor blade structure.

Figure 11b shows cross sections through corresponding sandwich plates.

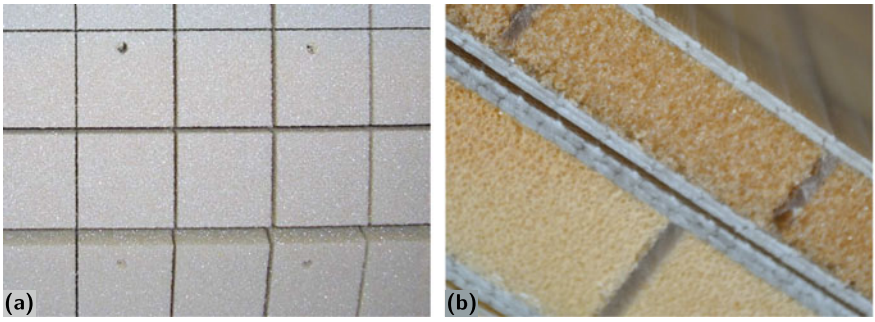

Fig. 11 Top view (**a**) of a PVC foam plate with a density of 60 kg/m^3, slotted and perforated, and sectional view (**b**) of sandwich plates with different thicknesses with GF-EP skins and PVC core; top 10 mm, bottom 15 mm thickness with partially filled slots;

4.6 Adhesives

The majority of the rotor blades manufactured nowadays are produced as two skin laminates. This means that the aerodynamic suction-side skin laminate and the aerodynamic pressure-side skin laminate are prefabricated separately. The shear webs which are needed are glued into one of the skin laminates and then the two skins are bonded together. The dimensions of the bonding partners mean that the bonding gaps which have to be bridged with an adhesive are large. In today's rotor blades, they are nominally specified to be around 5 mm, but can reach thicknesses of up to 30 mm. If they are to become structurally effective, the adhesive joints must not exceed a thickness of 10 mm. The adhesive exudes into empty spaces with thicknesses of up to the stated 30 mm in the region of so-called blind bonded joints as well.

Since the adhesives are usually exothermic-reaction resin materials, there is a risk of a significant local temperature increase, which can ultimately lead to the surrounding structure being damaged. Hence, the adhesive must also be kept as thin as possible even in regions which have no structural effect.

To be able to bridge thick bonding gaps as well, however, fillers are added to the adhesives. This increases the viscosity of the adhesives significantly. Depending on the type of filler selected, e.g. GF in the form of short fibres, the adhesive additionally becomes more or less abrasive during delivery and when mixing resin and curing agent. Finally, to simplify the workability during the process, thixotropic additives are admixed to the adhesives. Thixotropy describes the so-called shear-thinning behaviour. Shearing of the substance leads to a decrease in viscosity here. After a rest period, the viscosity increases again, however. This is important so that the adhesive does not slide off vertical surfaces again once it has been applied. One example for a thixotropic agent is pyrogenic silicon dioxide, also called pyrogenic silicic acid.

Further detailed information on adhesives and bonds can be found in [45].

4.7 Coating

A surface coating is applied to the rotor blade to protect its surface structure against weathering phenomena such as rain, ultraviolet (UV) light, sand storms, snow and ice. This coating usually consists of many different layers and can include the following:

- gel coat,
- putty,
- pore filler,
- finishing coat and
- erosion protection.

The gel coat is usually applied to the negative mould (see Sect. 8) of the rotor blade. The rotor blade structure is then stacked up inside this mould and bonds with

the gel coat layer during the manufacturing process. This provides the basis for the further surface processing of the rotor blade after it has been removed from the mould on the one hand; on the other, the gel coat forms a protection for the mould. Since the resin matrix has very low viscosity as a rule, it will also fill small depressions, defects and holes in the surface of the mould during the VI. After the curing, the resin is adhesively and mechanically bonded to the surface. Demoulding the rotor blade will then cause further damage to the surface of the mould. These mould surfaces must then be repaired on a regular basis. If the first layer in the mould is a gel coat, this bonding does not take place as just described and the mould surface is protected and accordingly has a longer life.

After the rotor blade has been demoulded, the surface is sanded to remove residues of the mould release agent from the production process and activate the surface for the application of the surface coating. Afterwards, any depressions are evened out with the putty and surface finished by sanding. The surface is then skimmed with the filler to fill the remaining pores. Lastly, the finishing coat is applied. The number of coating layers depends on the coating system used and the layer thickness to be achieved. The next step is to apply the erosion protection for the leading edge of the rotor blade. This can be an adhesive film or also a coating. Finally, aerodynamic aids such as vortex generators and trailing edge serrations are bonded to the surface.

Conventional gel coats consist of PU or EP. In general, PU in liquid form or in the form of a paste is used for the subsequent coating components, since it is characterised by good UV light resistance.

4.8 Metals

Metals are used in rotor blades for the lightning protection system, for the connection of the rotor blade root to the blade bearing of the rotor hub, and also at segmented-blade connections.

For the lightning protection system, a distinction is usually made according to the material used for the main reinforcements or spar caps of the rotor blade. GF composites act as a dielectric and therefore do not have to be protected separately. In these blades, the lightning protection system is limited to inserting contacted lightning receptors in the vicinity of the blade tip. The tip is especially endangered by potential lightning strikes because of its exposed position. The receptors to be inserted and the connecting lightning protection cable are made of aluminium because of its low specific mass. Since aluminium has comparatively poor fatigue strength, the aim is to lay the lightning protection cable along the lines of the elastic centres of the blade cross sections as far as possible (see Fig. 13).

If CF is used in the main spar caps (see Fig. 16a), solving the lightning protection problem becomes more difficult. The conductivity of the spar caps and their flammability means they have to be protected against lightning strikes in particular. Aluminium should not be used for this purpose, however, because contact corrosion can occur between CF and aluminium. Copper is therefore preferred here.

Furthermore, the lightning protection system is connected to the rotor hub via a slipring in some cases. This is then usually manufactured from stainless steel, for example, V4A.

Finally, high-strength tempered steels are used for the rotor blade connection to the blade bearing. The materials used for the expansion bolts achieve strength values in the region of 1000 MPa. Examples are 30CrNiMo8, 34CrNiMo6, 42CrMo4, 42CrMoS4 or 32CrB4.

5 Structural Models

Structure and substructure models of the rotor blade with various degrees of detail are used on the one hand to compute cross-sectional properties which are then used to parametrise beams for the load simulation, and on the other to carry out structural analyses with the computed loads. Since the design process and the optimisation are done iteratively, the computational efficiency of the models is particularly important. In a subsequent development stage, models which are more complex and hence more computationally intensive are relevant for detailed analyses.

The computationally efficient models include analytically based descriptions, and also semi-analytical descriptions with a relatively small number of variables to be determined. The computationally intensive models include detailed representations of the structure as shell and solid models, discretised with the aid of FE.

5.1 Geometry and Structure

The external geometry of the rotor blade, also called planform, results from aerodynamic and also structural requirements. Airfoils which are relatively thin have better aerodynamic properties than relatively thick airfoils. On the other hand, relatively thick airfoils allow more economical use of material, since the parallel-axis component in the geometric moment of inertia comes into play here. A challenge with the structural design is the transition from the airfoil of relatively long chord lengths to the cylindrical blade root at the connection. This is down to the large three-dimensional change of the rotor blade surface which leads to effects which cannot be described sufficiently well with first-order approaches. The changes in the cross sections along the longitudinal axis lead to so-called “pumping” or “breathing”, where the cross section deforms and it can no longer be assumed that the planarity of the cross section is maintained.

The rotor blade planform can be described by a family of airfoils, a chord length distribution, an aerodynamic twist distribution, a thickness distribution and a thread point distribution (Fig. 12). The airfoils are then usually characterised with respect to their aerodynamic lift and drag factors as a function of the angle of attack, see Fig. 3 in Chap. 4 of this book. Panel codes such as XFOIL [28] and its extension

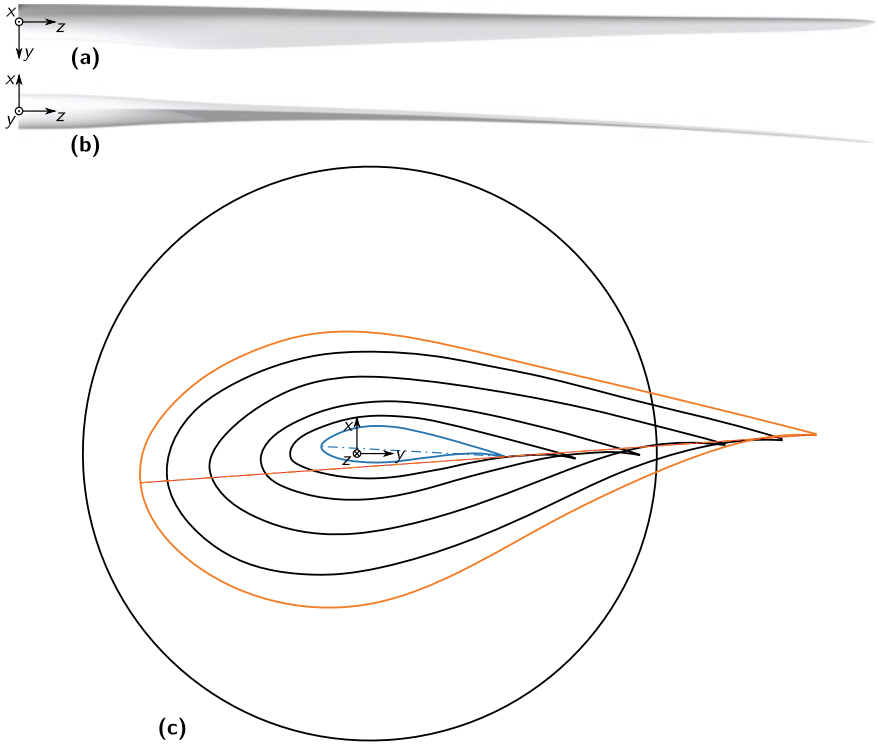

Fig. 12 Planform of a modern rotor blade of an onshore WTG: View onto the suction side (**a**), the trailing edge (**b**) and from the root into the inside of the blade (without pre-bend) (**c**); z-axis of the coordinate system marks the pitch axis; dash-dot line shows a chord of an airfoil close to the blade root and to the blade tip. Copyright © 2021 TPI Composites Inc.

RFOIL [10] or CFD codes such as OpenFOAM [30] or EllipSys [19] are used for this purpose. The aerodynamic performance is then analysed with the aid of BEM codes such as CCBlade [86, 89], QBlade [124] or FOCUS6 [145].

Load-bearing spar caps and webs are positioned within this geometric shell. Panel sections are built in sandwich construction, see Fig. 16. The manufacturing process is taken into account here.

5.2 Cross-Sectional Properties

When the distribution and positioning of materials within the blade cross section and in the longitudinal blade direction are known, the cross-sectional properties can be determined.

The structural properties of a cross section are described by a stiffness matrix and a mass matrix. Typically, the cross-sectional stiffness is given as a 6×6 matrix in accordance with Timoshenko beam theory [129]. For balanced laminates, this results in the following structure of the stiffness matrix $[S]$ in relation to a reference point in a reference coordinate system (CoS) (see Fig. 12) within the cross section:

$$\overrightarrow{F} = [S]\,\overrightarrow{u} \quad \Rightarrow \quad \begin{Bmatrix} F_x \\ F_y \\ F_z \\ M_x \\ M_y \\ M_z \end{Bmatrix} = \begin{bmatrix} k_x GA & k_{xy} GA & 0 & 0 & 0 & S_{16} \\ k_{xy} GA & k_y GA & 0 & 0 & 0 & S_{26} \\ 0 & 0 & EA & S_{34} & S_{35} & 0 \\ 0 & 0 & S_{34} & EI_{xx} & EI_{xy} & 0 \\ 0 & 0 & S_{35} & EI_{xy} & EI_{yy} & 0 \\ S_{16} & S_{26} & 0 & 0 & 0 & GJ \end{bmatrix} \begin{Bmatrix} \gamma_x \\ \gamma_y \\ \varepsilon_z \\ \kappa_x \\ \kappa_y \\ \theta_z \end{Bmatrix}, \tag{5}$$

where $\overrightarrow{F}$ contains the forces F and moments M acting on the cross section and $\overrightarrow{u}$ the shear strain γ, strain ε, curvatures κ and twisting θ. The shear centre relative to the reference point is given by [34]:

$$x_\mathrm{s} = -\frac{C_{26}}{C_{66}} \quad \text{and} \quad y_\mathrm{s} = \frac{C_{16}}{C_{66}}, \quad \text{where} \quad [C] = [S]^{-1}. \tag{6}$$

The elastic centre or centroid relative to the reference point is given by [34]:

$$\begin{Bmatrix} y_\mathrm{e} \\ -x_\mathrm{e} \end{Bmatrix} = -\begin{bmatrix} C_{44} & C_{45} \\ C_{45} & C_{55} \end{bmatrix}^{-1} \begin{Bmatrix} C_{34} \\ C_{35} \end{Bmatrix}. \tag{7}$$

The structural twist angle between the elastic axes and the reference CoS is given by [40]:

$$\nu = \frac{1}{2} \tan^{-1}\left(-\frac{2EI_{xy}}{EI_{xx} - EI_{yy}}\right). \tag{8}$$

To populate the stiffness matrix, the axial stiffness AE, the shear stiffnesses kGA, the bending stiffnesses EI and the torsional stiffness GJ are calculated. If structural couplings exist, e.g. between bending and torsion, these need to be determined as well. The fully populated stiffness matrix results only when unbalanced laminates are used. For the fully populated stiffness matrix, the shear centre additionally depends on the bending torsional compliances C_{46} and C_{56} [34], for example.

To consider the simplified concept it is often sufficient to determine the 3x3 sub-stiffness matrix comprising tension (AE) and bending components (EI) according to Euler-Bernoulli [31].

The populated mass matrix $[M]$ is then:

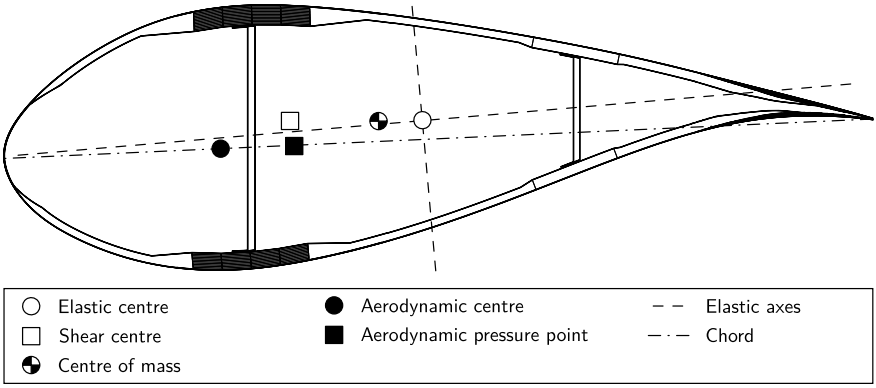

Fig. 13 Blade cross-sectional properties. Copyright © 2021 TPI Composites Inc.

$$\overrightarrow{F} = [M]\,\overrightarrow{\ddot{u}} \quad \Rightarrow \quad \begin{Bmatrix} F_x \\ F_y \\ F_z \\ M_x \\ M_y \\ M_z \end{Bmatrix} = \begin{bmatrix} m & 0 & 0 & 0 & 0 & M_{16} \\ 0 & m & 0 & 0 & 0 & M_{26} \\ 0 & 0 & m & M_{34} & M_{35} & 0 \\ 0 & 0 & M_{34} & J_{xx} & J_{xy} & 0 \\ 0 & 0 & M_{35} & J_{xy} & J_{yy} & 0 \\ M_{16} & M_{26} & 0 & 0 & 0 & J_{zz} \end{bmatrix} \begin{Bmatrix} \ddot{u}_x \\ \ddot{u}_y \\ \ddot{u}_z \\ \ddot{\theta}_x \\ \ddot{\theta}_y \\ \ddot{\theta}_z \end{Bmatrix}, \tag{9}$$

where $\overrightarrow{\ddot{u}}$ contains the accelerations $\ddot{u}$ and angular accelerations $\ddot{\theta}$. The location of the centre of mass is given by

$$x_\mathrm{m} = \frac{M_{34}}{m} = -\frac{M_{16}}{m} \quad \text{and} \quad y_\mathrm{m} = \frac{C_{35}}{m} = -\frac{M_{26}}{m}. \tag{10}$$

To populate the mass matrix, the masses are m and the moments of inertia J.

The stiffness and mass matrix elements are computed on the basis of a 2D discretisation of the cross section with arbitrary degree of detail (Fig. 13). The resulting grid can then be analysed with the aid of analytical methods [70, 140, 147] or numerically based methods, such as Variational Asymptotic Beam Sectional analysis (VABS) [14], BEam Cross section Analysis Software (BECAS) [8], Sonata/ANBA4 [32], PreComp [7] or Farob/FOCUS6 [76, 145]. The methods have different requirements regarding the grid quality.

5.3 Beam Models

When modelled as a beam, the rotor blade allows for a computationally efficient analysis of global properties such as resonance frequencies (also called natural frequencies or eigenfrequencies) and modes, determination of total mass and the overall

centre of mass as well as the analysis of the deformation response to arbitrary external load cases.

The classic beam according to Euler-Bernoulli [31] uses only the tension and bending components of the stiffness matrix. An implementation can be found in [48]. Such a beam is implemented in ElastoDyn as part of OpenFAST, for example. For computationally intensive processes, the degrees of freedom of the beam are significantly reduced by using modal correction methods. This method is clearly illustrated in [37]. The theory according to Timoshenko [129] additionally takes account of shear and torsion components as well. Extended beam models take account of all structural couplings, i.e. a full 6x6 stiffness matrix (Eq. 5) as well as geometric non-linearities. Such a beam is implemented in Geometrically Exact Beam Theory (GEBT) [53], BeamDyn [137–139] as part of OpenFAST or in the form of an anisotropic beam element [69] in HAWC2, for example. The implementation of the beam in the form of FE in environments such as Ansys APDL [2] has turned out to be beneficial for the design of full-scale blade tests [81]. Modal correction methods can no longer be applied to geometrically non-linear considerations.

A comparison of different degrees of detail for beam models with impact on the WTG loads resulting from aero-servo elastic simulations can be found in [102].

5.4 Models for Thin-Walled Structures

Rotor blades are thin-walled structures, i.e. the wall thickness or skin thickness is relatively small compared to the thickness of the rotor blade. The elongation across the skin thickness can therefore be assumed to be constant. Simply supported or clamped plate or sandwich models [141] are therefore suitable for the stability analysis of parts of the cross section such as shear webs, spar caps or panel sections, and also for the strength analysis of adhesive joints. The stiffnesses of a structural part are described using CLPT, see Sect. 4.4. The total cross section can also be modelled as the chain-linking of plate and sandwich elements, however, so that a stability analysis on the cross-sectional level becomes possible. In so-called finite strip models, a thin-walled cross section is modelled with prismatic discretisation. A rotor-blade-specific implementation is known as FINSTRIP [133].

A comparison of different models for the stability calculation can be found in [105].

5.5 Full-Blade and Detailed Models

Beam models based on structural properties that are uniform across a beam element and prismatically discretised are sufficient for less detailed estimates of the structural response, such as elongations along the blade trailing edge. When, for example, planar elongation states are of interest, however, FE models are indispensable. This

is particularly relevant in the tapering and geometrically twisted section inside the blade which transitions from a circular cross section to an airfoil and whose cross-sectional deformation can no longer be described with beam models.

FE models of the full blade are often based on shell elements which are based on first-order shear deformation theory [101]. This makes it possible to consider shear stiffnesses in the thickness direction and turns out to be advantageous in the stability analysis of local effects in sandwiches [107]. Solid elements which are coupled to the shell can be used for the analysis of adhesive joints [109]. The use of solid elements allows normal stress components in the thickness direction to be considered in addition. This can be helpful in the analysis of thick laminates, particularly near the blade root. To avoid the enormous increase in computational effort [106] when modelling the full blade as a solid model [93, 94], it is worthwhile creating detailed substructure models. In submodelling, node displacements and rotations of the full-blade shell or solid model are transmitted to the cutting interfaces of the submodel.

A detailed model is often used for the analysis of the blade root connection or segmented-blade connections, to include the eccentric loading of the expansion bolt and the laminate, for example, see Sect. 6. The same applies to adhesive joints which are subjected to a multi-axial internal load.

6 Blade Root Connection Concepts

Two concepts have essentially been successful for the blade root connection: the joint with bushing (or insert) and with T-bolt, see Fig. 14.

In the bushing joint, an expansion bolt clamps the inner ring of the blade bearing to a bushing bonded to the blade root laminate. The axial longitudinal force of the bolt is transferred from the outside of the bushing to the inner and the outer root laminate via shear forces. The bushing is accordingly designed to be long so that sufficient surface area is available for the shear force transfer.

With the T-bolt joint, the expansion bolt clamps the inner ring of the bearing to the root laminate. The axial longitudinal force of the bolt is transferred from the barrel nut to the pre-tensioned laminate through a positive mechanical and frictional engagement. The laminate section between two adjacent barrel nuts (not shown in the figure and subsequently referred to as the net section) then transfers the longitudinal force to the root laminate.

The cross-sectional view leads one to suspect that the connection is subject to eccentric loading. In the bolt in particular, this causes a bending load in addition to an axial one. The form of this internal load in the longitudinal direction, and also along the circumference of the root, depends on the compliance of the hub, the blade bearing and the concept for the blade root connection [15, 113].

The use of bushings in the root tends to allow the root region to be designed with thinner walls than for roots with T-bolt design. A motivation for the structural preference of bushings could therefore be a lower blade mass, which would then be reflected in a reduction of the loads in blade bearing, hub and tower. The complexity

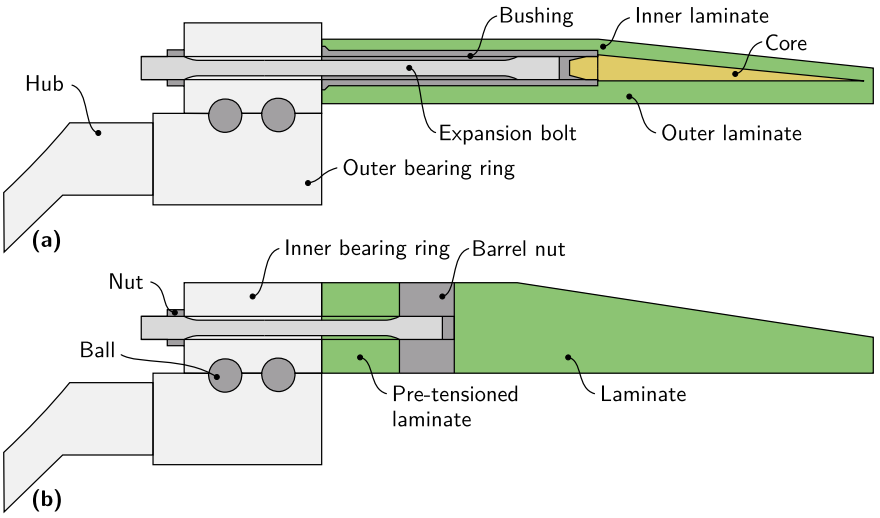

Fig. 14 Cross-sectional view through the blade root connection, constructed using a bushing (**a**) and a T-bolt (**b**). Copyright © 2021 Malo Rosemeier

of the bushing connection means that a computational structural analysis is associated with a great amount of modelling and validation effort. In practice, the permissible extraction force is often determined experimentally with an axial extraction test of a unit cell. This has the disadvantage that a design of a bushing connection is usually retained for each new blade design and accordingly only the root diameter and hence the number of bushings is adjusted. When the wall thickness remains constant, the relative wall thickness decreases, which favours cross-sectional deformations such as the so-called "breathing". This "breathing" can cause unfavourable internal loads in sandwich panels and in the blade bearing.

Analytical models to assess the limit states of the T-bolt connection, such as net section failure, bearing failure, shear-out failure and cleavage failure [26, 116] are established, however, as is the CLPT for thick laminates in particular [16]. The advantage here is that the T-bolt connection can be optimised in detail for every new blade design, see also Sect. 9.4.

7 Structural Design Verifications

The ultimate and fatigue strength verifications for the structural members subjected to the design load cases are conducted in accordance with the certification scheme selected, i.e. the partial safety factors to be used. In addition, further verifications which affect the serviceability of the WTG have to be conducted in relation to the rotor blade structure.

7.1 Strength Verifications for Fibre-Reinforced Polymers

To assess the load-bearing capacity of rotor blades for WTGs, it is first necessary to know the strengths of FRPs. The materials testing (Sect. 4.3) usually provides this information only for UD-NFC composites or for UD single plies, however. The orthotropy of FRPs means that a direct assessment of the load-bearing capacity is not possible. Hence, the use of failure criteria and failure functions has become normal practice. For the ultimate strength verification of rotor blade structures, the procedure according to PUCK [98, 135] is now established.

The strength hypothesis according to PUCK is an action-plane-based failure model. It is based on the COULOMB-MOHR strength hypothesis, which was originally developed for geodetic materials and heaps of material. It produces realistic strength predictions especially for the quasi-static compressive load transverse to the fibre direction. To this end, the failures are first categorised into fibre-dominated (fibre fracture (FF)) and matrix-dominated failures (inter-fibre fracture (IFF)). Furthermore, a distinction is made between the fracture modes A, B and C of the IFF.

- FF: Failure caused by a tensile or compressive stress in the fibre direction.
- IFF Mode A: Failure caused by a combined tensile and shear stress which acts in the direction of the tensile stress perpendicular to the fibre direction.
- IFF Mode B: Failure caused by a combined compressive and shear stress which acts in the direction of the compressive stress perpendicular to the fibre direction, where the absolute value of the shear stress is greater than the absolute value of the compressive stress.
- IFF Mode C: Failure caused by a combined compressive and shear stress which acts in the direction of the compressive stress perpendicular to the fibre direction, where the absolute value of the shear stress is less than the absolute value of the compressive stress.

When used as part of the structural optimisation, this has the advantage that it is possible to identify the stress or load state which was the original cause of the failure as well as the component, fibre or matrix which failed. In addition, the expression according to Puck is homogeneous of degree one. This means that stress exposures can be stated in the form

$$e = \frac{[\sigma]}{[R]}. \tag{11}$$

The stress exposure e is then linearly dependent on the stress vector $[\sigma]$ of the single ply. $[R]$ is a strength vector. An actual division only works in the uni-axial case, however, while the mathematical effort is higher for complex stress states. Details are given in [98]. The consequence of the linear dependence is that for a stress exposure of $e = 0.5$, a load precisely twice as large would lead to failure.

Moving on to the fatigue strength analysis, it turns out that predictions are not possible without further ado with PUCK's failure hypothesis, since a superposition of the stress exposures from different fracture modes and fibre stress exposures is

not covered. Hence the fatigue strength verification is frequently based on results of fatigue strength tests on the coupon level of the testing pyramid (Fig. 1).

A WTG easily experiences load cycle numbers of around $n = 10^8$, which already originate simply from the number of revolutions of the rotor as a consequence of rated operation. This load cycle range is the so-called Ultrahigh-Cycle Fatigue (UHCF) regime.

The fatigue strength properties of FRPs depend on many parameters. The first step is to describe their phenomenological behaviour under service loads in the different phases.

It is observed that FRPs initially have no macroscopically visible damage under this type of load when the loads are sufficiently small. This phase ends when the first crack occurs in the FRP as a consequence of the load, usually in the matrix or the fibre-matrix interface. At the same time, this point in time marks the transition to the phase of crack density growth. In this phase, the mechanical properties of the FRP degrade to a greater or lesser extent. The incidence of the initial damage and the crack density growth are affected significantly by the stacking of the semi-finished textile materials, for example, by the crossing points of fibres lying on top of each other as well as the arrangement of the stitching threads, for example [146]. The total failure of the composite ends this phase as well as the fatigue process overall.

Depending on the size of the load and the orientation of the reinforcing fibre in the composite in relation to the load direction, the overall process proceeds with different speeds [78]. It can lead to failure within only a few thousand load cycles or last for millions of load cycles.

It is easy to understand that the sizing, whose purpose is to ensure the bonding between fibre and matrix, has a significant effect on the point in time of, and the stress level at damage initiation, and thus on the fatigue strength behaviour [127]. In consequence, the matrix also has a substantial influence on the damage initiation in FRPs, especially when the load direction is arranged transverse to the fibre direction [78].

In addition to the mechanical properties, also as a function of temperature and the degree of curing [3, 33], the visco-elastic behaviour, such as the strain rate dependence, creep behaviour and relaxation behaviour [79, 83] and the fracture toughness [123] of the matrix also have an influence on their fatigue strength behaviour. A matrix-based procedure therefore works quite well, at least to predict the initiation of matrix-dominated damage [74]. In this procedure, a comparison stress is formed on the component level, which makes the consideration independent of the reference planes used by PUCK.

The fatigue strength behaviour of polymers can be quite simply expressed using the equation according to BASQUIN [4]. The results of changing tensional-compressive loads with the load ratio of $R = -1$ are quite well simulated by this at least. The load ratio is defined by

$$R = \frac{\sigma_l}{\sigma_u}, \tag{12}$$

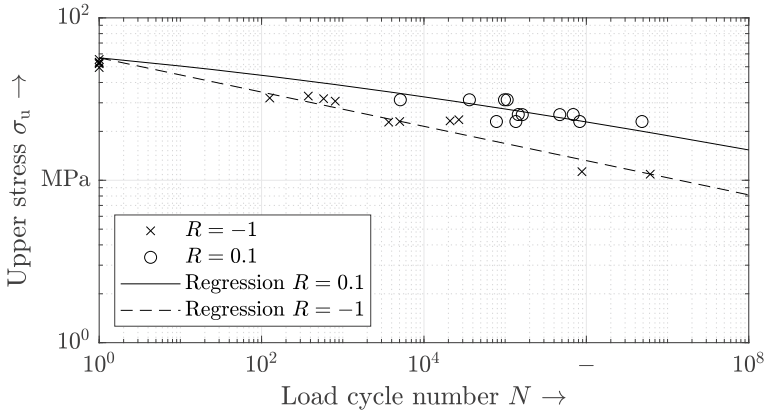

Fig. 15 Results of the cyclic test and regression according to BASQUIN-GOODMAN for an EP adhesive. Copyright © 2021 Alexander Krimmer

where the index u stands for the upper and the index l for the lower stress of a sinusoidal internal load.

Further detailed information on the fatigue strength test and the fatigue strength in general can be found in HAIBACH [46] and SURESH [121]. In combination with the equation according to GOODMAN [43], load conditions deviating from $R = -1$ can be described as well. Corresponding experimental results and regressions for the approaches given are shown in Fig. 15 for an adhesive. The test results for $R = -1$ and $R = 0.1$ were evaluated in their entirety here. The corresponding curves shown are based on the same parameter set with the negative inverse stress-life exponent $m = 9.48$ and the strength $R_t = 56.8\,\text{MPa}$. The graphs presented can be generated with [104]:

$$N = \left(\frac{2R_t}{(1-R)\,\sigma_u} - \frac{|1+R|}{1-R} \right)^m . \tag{13}$$

With some restrictions, the approaches can be transferred to FRPs as well. An isotropic adhesive was used here to make the illustration clear and intelligible. Moreover, further approaches to the description are conceivable [104].

7.2 Stability Verifications

The stability of a structure is essentially determined by its stiffness and slenderness. If a load-bearing structure becomes unstable, this leads to a sudden deformation, which then usually leads to a strength failure. For rotor blades, a distinction is made between global and local stability failure (also called buckling failure). Global buckling takes

place when, for example, a sandwich becomes unstable in its entirety, comprising the skins and the core. In practice, the sandwich then behaves like a plate made from a single laminate ply. Local buckling is when the skin becomes unstable because of skin wrinkling, for example, or the core becomes unstable because of core shear crimping, for example [107]. Details of various stability failure modes can be found in [141]. Local modes can be described well with analytical models, see Sect. 5.4. Within limits, the frequently used FE shell model with adequate element types is used for this purpose as well, however, see Sect. 5.5.

For the verification, the solutions of a linear eigenvalue problem, i.e. the buckling resistances and their buckling modes, are compared to an applied extreme load distribution and expressed with the safety reserve factor (Eq. 4). Since rotor blades are thin-walled on the one hand and slender, strongly deforming structures on the other, a computationally much more complex geometric non-linear stability analysis which takes account of geometric imperfections, i.e. the application of stress-free pre-deformations, can be carried out, where the load vectors follow the deformation step by step [106].

7.3 Verifications of the Adhesive Joint

Adhesive joints in rotor blade structures are subjected to both mechanical internal loads caused by gravitational loads and aerodynamic actions as well as internal loads caused by a change in temperature. In addition, these loads are multi-axial, comprising linear expansion, shear and peeling. In principle, the ultimate strength verification as well as the fatigue strength verification for the adhesive joint can be carried out along the lines of the IFF of FRPs on the basis of stress-based methods [109], see Sect. 7.1. For the purpose of model validation, tests can be carried out on the coupon level, and also on the full-blade level or an intermediate level of the testing pyramid (Fig. 1).

At first sight, the frequently observed transverse cracks in rotor blade adhesive joints do not seem to have any effect on the integrity of the blade structure and a damage-tolerant design could be discussed here, cf. [67]. However, since the consequences of initiated transverse cracks, such as crack propagation into the load-bearing structures [109], can lead to an increased failure probability, a safe-life design seems to be the right approach to achieve reliable operation.

7.4 Verifications of the Sandwich Core

Relatively wide and thin-walled sandwich panels, particularly inside the blade near the root, are exposed to the so-called “breathing”, a deformation within the cross section. This means that bending takes place in the sandwich in addition to the axial tension. Here, the core is subjected to a shearing load in a plane of the plate across

the thickness and a compressive load out of the plane of the plate. The verifications are provided with suitable plate or detailed models, see Sects. 5.4 and 5.5.

7.5 Verifications of the Expansion Bolt

The preloaded expansion bolt at the blade root connection or at a segmented-blade joint is one of the few replaceable load-bearing structural members of the rotor blade. The eccentric load situation at the blade root connection (see Sect. 6) causes a bending stress of the bolt as well as the purely axial load. As a machine element, the verifications for the expansion bolt are provided on the basis of recognised mechanical engineering guidelines such as [134], for example.

7.6 Serviceability Verifications

In addition to the verification of critical deformation, i.e. the tower clearance between blade tip and tower surface in particular, verification must be provided that the resonance frequencies of the rotor blade are not excited by the rotor frequency and its harmonics which arise in operation. For this purpose, the rotor blade can no longer be considered separately from the WTG system, since the resonance modes between the blades occur in so-called coupled rotor modes, cf. [117]. Such a verification is provided with the aid of a Campbell diagram, see Fig. 7 in Chap. 7 of this book. In addition, mention is also made here of the verification of aero-elastic instabilities, such as flutter [47] and vortex-induced vibrations of the rotor blade [51].

8 Manufacturing

Rotor blades for WTGs are usually manufactured in negative moulds for the rotor blade skins. These moulds define the aerodynamic skin of the rotor blade for the manufacturing process, which is then filled with the rotor blade structure during the manufacturing process.

Most rotor blades manufactured today are produced as two skins. These blades therefore comprise two load-bearing skins for the aerodynamic suction side and pressure side, into which the main reinforcement is integrated. The two skins are joined together by means of structural adhesive joints and via shear webs to form the final rotor blade structure. A corresponding rotor blade cross section is depicted in Fig. 16a. The adhesive joints of the leading edge, the trailing edge and the shear webs in the aerodynamic pressure side are marked accordingly. In the aerodynamic suction side, the connections of the shear webs were carried out as HL in this case.

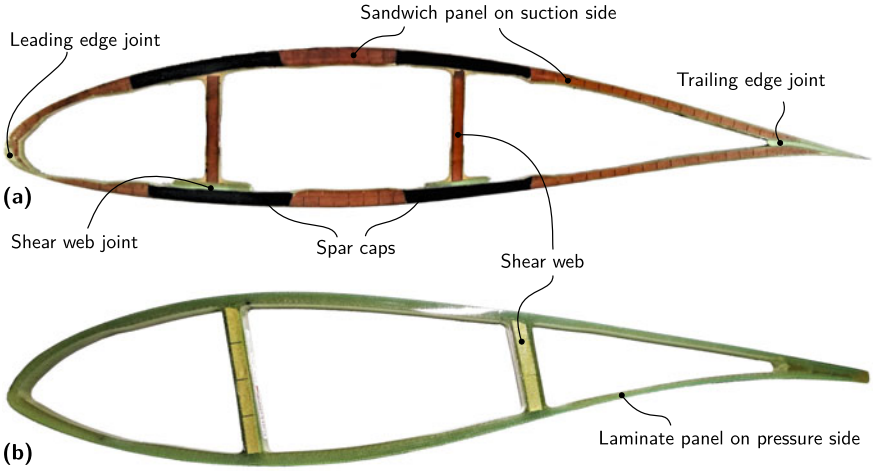

Fig. 16 Blade cross section from a rotor blade in half-shell construction with four spar cap system and CF-reinforced spar caps (**a**) and from a One-Shot blade manufactured by means of integral construction by CARTFLOW (**b**). Copyright © 2021 Alexander Krimmer

Furthermore, it is possible to identify the spar caps, which are shown in black because of the CF reinforcement and arranged here in a four spar cap system.

Deviating from the half-shell construction, rotor blades are in some cases manufactured by means of so-called integral construction. Siemens Gamesa Renewable Energy (SGRE) in particular developed the IntegralBlade® technology [120], as it called it, and established it even for rotor blades on large offshore WTGs. Another manufacturer which pursues a similar approach is CARTFLOW. A rotor blade cross section of a blade from this manufacturer is illustrated in Fig. 16b. Here, the lack of a structural bond is particularly conspicuous.

In Sect. 8.1, the discussion first addresses the most important manufacturing processes used in rotor blade manufacture. Sect. 8.2 provides an overview of possible constructional deviations and their consequences.

8.1 Methods

For rotor blades, a fundamental distinction is made between the manufacture of rotor blades with the HL method, with the method using pre-impregnated fibres (prepreg), and the VI method. In all cases, single-sided moulds are used, which are sealed in different ways. Essentially, these three methods differ in the way the resin matrix is introduced.

In VI manufacture, which covers many different methods such as Vacuum-Assisted Resin Infusion Moulding (VaRIM) and Seaman's Compound Resin Infu-

sion Moulding Process (SCRIMP), a vacuum bag is applied onto the dry stacked-up semi-finished fibre material. This is then evacuated with vacuum pumps before the low-viscosity resin matrix, which follows the largest pressure gradient, is pressed into the component.

If the manufacturing process still uses the HL method, these steps are mainly limited to overlaminates, which are usually applied throughout the finishing process or in the course of repairs if manufacturing deviations have to be corrected. However, it is essential here that a predefined quantity of resin is applied to the semi-finished fibre material outside the mould. This can also be done with an automated impregnating machine.

After impregnation, the work steps in the prepreg and HL methods are nearly the same. The work sequence for the VI method is now briefly described.

Even today, the manufacture of rotor blades for WTGs is still largely a manual process. The layup of the non-crimped textiles and the core material is usually done by hand. Prefabricated components are placed into the rotor blade mould with the aid of hoists or cranes. The flow media, feed lines and suction hoses as well as the vacuum bag are again arranged by hand. The vacuum is produced by vacuum pumps to a differential pressure of approximately atmospheric pressure. The stacked setup is then checked for leaks. Once this has been done, the infusion can commence.

Before the infusion, the heater, which is usually integrated in the rotor blade mould, is brought to a predefined processing temperature. After the infusion is completed, the temperature is increased to a material-dependent value and maintained at this value to ensure the resin matrix is cured. During curing, the resin matrix undergoes volumetric shrinkage. The more the viscosity of the resin material increases, the more it is able to transfer shear forces. The shrinkage component, which can transfer forces, is called polymer-physical shrinkage. This causes internal stresses, which are comparable to thermal residual stresses [115].

Blades manufactured in integral construction are removed from the mould and after curing, they are practically ready for the surface finishing and post-processing of the blade root connection. In contrast, the two blade skin laminates and the prefabricated shear webs are joined by bonding, trimmed, overlaminated and then subjected to surface finishing as well as post-processing of the blade root connection. The process of half-shell manufacture is nicely illustrated in a video [130].

8.2 Deviations

Within the processes described, the structural properties can naturally deviate from the desired state. A distinction must be made according to whether these are deviations which lie within the tolerances specified or outside them. When they lie within the tolerances, then the effect of the deviation on the serviceability and operational safety of the rotor blade structure is taken into account in its design and is acceptable. If a deviation is outside the tolerances specified, then the serviceability and operational safety of the structure may possibly be compromised. The design engineer

can examine this by computation. If the structure is not operationally safe and not sufficiently load-bearing, the deviation must be remedied. In general, this means a repair of varying degrees of complexity.

Examples of these deviations are

- air inclusions (finely dispersed air bubbles, local accumulations of air or even dry spots in the laminate);
- undulations (angle errors, waviness or wrinkles in the laminate);
- misalignments (insufficient overlaps, gaps between plates of core material);
- cracks caused by internal (for example, temperature-related) stresses;
- uncured material (caused by mixing errors or insufficient heat input during curing) and
- discolourations or changes to the mechanical properties caused by local overheating especially of the core material.

If a repair is not carried out, the consequences for the support structure can sometimes be disastrous. The consequences of the deviations are presented in brief here.

Air inclusions primarily affect the matrix-dominated properties of the composite. This means the matrix-dominated moduli and strengths decrease with increasing porosity, for example. This is particularly critical for the compressive strength in the fibre direction, since the matrix provides less support to the fibres.

Undulations right through to waviness and wrinkles primarily affect the compressive strength of the laminate in the fibre direction. A misalignment of the fibres causes the stresses to transfer from the fibres into the matrix. The stresses which a matrix can tolerate are much lower than those which the fibres can tolerate. Hence undulations sometimes cause drastic decreases in the compressive strength in the fibre direction. Undulations, especially in main reinforcement elements such as spar caps, are generally extremely critical deviations.

Misalignments usually lead to excessive stresses at overlaps or in the adjacent structural members. They can occur in all parts of the structure and are to be assessed as being critical.

Cracks are not always directly critical for the operational safety. They do lead to the formation of voids in the structure, however. These can fill with moisture, for example, under certain weather conditions and frost can then aggravate the damage, for example. In any case, they form the starting point for damage growth.

Uncured material is extremely critical to the operational safety of FRP structures. The transfer of forces from fibres to matrix and vice versa is only possible to a limited extent. This means that the fibre-dominated and the matrix-dominated strength is compromised.

Discolourations indicate a change in the chemical and therefore potentially the mechanical properties. In the case of core materials, the buckling stability of sandwich structures may be compromised here.

9 Topology Optimisation

Now that all the important components of the rotor blade and their mechanical properties are known, a structural optimisation is possible. For the optimisation, a quantity needs to be specified which can be used to assess the quality of the design. This is then minimised or maximised during the optimisation. In a lightweight construction such as a rotor blade, the mass is an obvious optimisation target, which of course has a crucial impact on the loads of a WTG since it is a cantilever beam structure.

The usual procedure is to carry out a load simulation with an initial model draft of a rotor blade. In relation to the wind turbine, the rotor blade is described by its stiffness distribution, its mass and its static moment. The objective is to demonstrate by means of computation the load-bearing capacity and operational safety of the rotor blade in all aforementioned verifications with the loads determined from the load simulation.

For a WTG, costs, yield and the LCoE are assessment parameters of overriding importance. Since the rotor blades account for between 15 and 25 % [99] of the wind turbine costs, the rotor blades have a significant influence on the aforementioned assessment quantities. It is difficult to optimise the WTG as an overall system, however, since the rotor blade designer often does not have all the necessary information about the turbine at their disposal. For simplicity, the optimisation is therefore restricted to a rotor-blade-related optimisation.

When, in the course of the optimisation, the mass and the static moment of the rotor blade deviate from the rotor blade model initially used for the load simulation, a new load simulation must be carried out. According to [60], tolerances of $\pm 3\,\%$ and $\pm 4.5\,\%$ apply to the mass and the static moment of the rotor blade, respectively.

An overview of possible optimisation targets and their interaction is given below. Guidance is given for taking aero-elastic effects into account. Greater emphasis is nowadays being placed on optimisation of design for manufacture in particular, since it has a significant influence on the quality and the manufacturing cycle time.

9.1 Optimisation Targets

As already mentioned, the optimisation targets according to which the rotor blade is optimised may differ or supplement each other. These targets can be

- energy yield,
- costs,
- mass,
- loads and
- power.

The primary objective of the design is naturally the generation of a high yield. Hence material which is as low cost as possible should be used. Basically, the topology of a structure is therefore optimised until it is no longer possible to achieve the

optimisation target with the given set of materials. Only at this stage does the change to a higher quality material take place, since this is generally accompanied by higher costs.

To be able to constructively assess these relationships, the important structural properties must be monitored during the optimisation. It is therefore advisable to create a mass model and a cost model for the rotor blade structure. This should include, for example, Capital Expenditures (CapEx) for material, production equipment and tools, staff, transport and in the best case even Operating Expenditures (OpEx) for maintenance and repair, for example, as well as Disposal Expenditures (DispEx) which are incurred by the rotor blade for the whole turbine. The yield model is usually provided by the aerodynamicists. They also answer questions regarding power and loads, cf. [65].

It is not always possible to directly assess the mass and cost impacts of adjustments on the structure. When changes are made to the structure, their consequences for the mass (Fig. 6) and the costs should therefore always be considered. With the structural and topological optimisation, it can be assumed that the yield initially remains the same. The steps mentioned mainly cover the issues of yield, costs, loads, mass and power.

Further boundary conditions may possibly also have to be taken into account in the optimisation. These can be

- time to market,
- manufacturing cycle time,
- quality,
- number of main moulds and additional moulds,
- recyclability,
- space required in production and
- transport restrictions (bridge height, radii of road bends and rail tracks).

All these topics should be considered when designing and optimising the rotor blade structure.

9.2 Aero-Elastic Properties

The blades become more slender with increasing rotor blade length. This can be attributed to the tip-speed ratios (TSRs) of the turbines on the one hand. They are sometimes simply equipped with longer blades, while the other turbine characteristics remain the same. This means that the tip-speed ratio in rated operation increases, which leads to more slender rotor blades, see Fig. 12 in Chap. 4 of this book. Furthermore, transport restrictions lead to slender blades, since the maximum chord length and the root diameter, for example, are restricted by boundary conditions for road or rail transport.

More slender blades are more susceptible to aero-elastic instabilities, since the enclosed area of a cross section has a significant influence on its torsional stiffness

and decreases from cross section to cross section in relation to the length of the rotor blade. This relationship is described by the second BREDT-BATHO formula and is a consequence of the first BREDT-BATHO formula, which assumes a constant shear flux in the cross section caused by the torsion [141]. For cross sections with inhomogeneous properties, the relationship is more complex [144], but the difference is small in the first approximation [5].

To counteract the tendency to aero-elastically unstable behaviour, it is primarily necessary to ensure that the shear centre (Fig. 13) of the cross section is located in the edge direction in front of the pressure point of the aerodynamic force at around 1/3 of the airfoil chord length so that the aerodynamic load causes a twisting of the cross section towards the feathering position, i.e. towards a smaller angle of attack. A twist towards a larger angle of attack has an unfavourable impact on the loading, for example, through stall-induced vibrations [47].

A further issue which can affect the aero-elasticity is the changing structural twisting angle along the rotor blade (Eq. 8). This is mainly caused by the fact that rotor blades have an aerodynamic twist, which means that the airfoils are arranged along the blade axis so that they always have the most favourable aerodynamic angle of attack. In Fig. 12b, the airfoil chords of the largest and the smallest airfoils are marked by dot-dashed lines. This makes it easy to see the different angles of attack. In Fig. 13, the main axes of inertia are furthermore marked by dashed lines. It is easy to imagine that the twist of the main axes of inertia roughly moves with the twisting of the airfoil chord, naturally influenced by the position of the main spar caps. This basically illustrates that a pure bending moment in the flapwise direction, for example, always causes a lead-lag bending as well.

9.3 Design for Manufacturing

Optimisation of the manufacturing cycle time, quality, number of main and additional moulds, space required for manufacturing and recyclability touches on the field of Design for Manufacturing (DfM). Here, the assessment is not as easy as for the pure structural optimisation, since the advantages and disadvantages in the manufacturing process are often not as easy to assess. It may be the case that a specific process can proceed faster, but that more staff need to be involved. Such a step would only be advantageous when the cost savings resulting from the shorter processing time overcompensate the higher staffing costs.

It is possible to formulate some rough guidelines, however. To keep the manufacturing cycle time short, a proven method is

- to keep the ply book simple;
- avoid local reinforcements, if possible;
- keep the number of prefabricated components low;
- keep the number of additional moulds correspondingly low and
- carry out manufacturing steps in the main mould, coordinated where possible.

Since main spar caps are usually manufactured in additional moulds, for example, it would therefore be favourable to decide for a two spar cap concept instead of a four spar cap concept, since fewer components will have to be manufactured in an additional mould. A structural comparison of the two concepts is provided by [105]. This means in practice that the main spar cap pair must be arranged where the airfoil is thickest, where the parallel-axis contribution to the flapwise bending stiffness is optimum. A less pronounced trailing edge spar cap pair, as shown in Fig. 13, provides lead-lag bending stiffness.

Attention is currently also being paid to the recyclability of rotor blade structures. To facilitate this, recyclability must already be taken into account when designing the rotor blade structure, in the selection of the materials and manufacturing processes, see Sect. 10.

9.4 Blade Root Connection

As has already been indicated in Sect. 6, as far as the blade root connection is concerned, the optimisation of the bushing connection is often limited to the adjustment of the diameter of the root circle and thus to the number of bushing segments over the root circle, because of the analysis effort involved. When upscaling, the wall thickness thus remains constant. This can lead to unfavourable cross-sectional deformations and thus internal loads, which cannot be counteracted in the construction without complex further development of the bushing connection. If the expansion bolt is the dimensioning element of the connection, however, the bushing connection allows a larger number of connection segments to be accommodated over the root circle than does the T-bolt connection, thus relieving the load on the expansion bolt.

It is comparatively easy to verify the failure modes of the T-bolt connection, in contrast. The essential parameters therefore remain available to influence the mechanical properties. These are, for example, laminate thickness, fibre angle, barrel nut diameter, net section fraction in the barrel nut circle, expansion bolt length, flange separation of the barrel nut bore and others. All these parameters can and must be optimised to guarantee the load-bearing capacity of the connection.

As already mentioned, the price is an important optimisation target. Here, the T-bolt connection has significant advantages over the bushing connection because the material costs are already much lower. The increased effort required to manufacture the bushing connection increases this advantage further. A disadvantage in this consideration is that the manufacture of the T-bolt connection requires a separate workstation for the rotor blade, which is situated between the main mould area and the area for the post-processing and the surface finishing of the rotor blade. Moreover, the drilling machine for the T-bolt connection has higher initial capital expenditure than the milling cutter for the milling finish of the bushing flanges once the rotor blade has been manufactured.

Especially because of the significantly lower costs for the T-bolt connection, it is necessary to make a well-justified decision for one or the other type of connection.

9.5 Blade Segmentation

Blade segmentation is a topic which is discussed time and again as a way to react to restrictions on the blade lengths to be transported. Blade segmentation means that the rotor blade is manufactured in two segments and provided with a connection at its separation point in a similar way and with similar versions as the root connection. The two segments are then joined together on the WTG construction site.

Blade segmentation is rarely used, however. Segmented blades were the standard design at ENERCON for a long time, but have been replaced by one-piece manufacturing despite the blades increasing in length. Other manufacturers also repeatedly experiment with the concept. If one type of rotor blade is manufactured for a large number of WTG types or sites, it can be worthwhile to produce various blade tip lengths which are then individually combined with a root segment to suit the requirement. It must be noted here that this procedure is not established practice as yet. Until now, the segmented manufacture of rotor blades has been more frequently used to solve logistical problems, at GENERAL ELECTRIC (GE) and SGRE, for example.

Disadvantageous is particularly the mass of the joint. It is smaller, the more the position of the segmentation joint is shifted towards the tip, since the forces and moments to be transferred decrease. Here they have a greater leverage with respect to the root, however, so that the mass of the joint is unfavourable for the static moment of the rotor blade.

It must be stated in general that the segmented manufacture of rotor blades primarily affects the logistics of the rotor blade. This normally comes before the actual service life of the rotor blade and only takes a few weeks of the rotor blade life. The compromise which has to be made for this has a negative impact on the structure in the form of additional forces and moments for the remaining service life of the rotor blade, which is between 20 and 30 years in operation. This must be counteracted with an additional support structure, which in turn increases the masses and thus the loads of the rotor blade. It therefore makes sense to consider whether it is not more favourable to find the technical solution in transport technology, since logistical solutions can be reused for many blades, while blade segmentations have to be built into each individual rotor blade.

10 Sustainability

"…to make development sustainable [is] to ensure that it meets the needs of the present without compromising the ability of future generations to meet their own needs" [131]. To safeguard sustainable development in this way, 195 countries have undertaken to limit the global temperature rise to significantly below 2 °C and to strive to keep it below 1.5 °C [132]. This limit allows the emission of only a limited amount of CO_2. According to the "budget approach" [100], this means a complete decarbonisation for Germany, i.e. CO_2 or climate neutrality by 2035 [100]. Climate

neutral here means that all fossil fuels have to be replaced with renewable energy sources by then.

As engineers working with wind energy, we are frequently confronted with the question as to whether wind energy can actually be converted with a smaller CO_2 footprint than energy from other sources of energy. Reference is made first to [114], which states that the CO_2 footprint for onshore wind energy is 11 gCO_2eq/kWh in the median. For offshore wind energy, the value is given as 12 gCO_2eq/kWh and is thus equal to the CO_2 footprint of nuclear energy. All other commercially available technologies are at least a factor of 2 higher. It must be stated, however, that the issues of the treatment of the waste from the nuclear energy conversion and repositories for this waste have still not been solved, even 70 years later [11], which is not compatible with sustainable development.

It is now possible to compare the above-mentioned values for the CO_2 equivalent of the energy sources with the CO_2 footprint of the current energy mix. For 2018, this has been given as 475 gCO_2eq/kWh [54]. It is clear that wind energy is currently the most favourable source of energy as far as the CO_2 footprint is concerned, and is significantly better than the current energy mix, but it does not yet achieve CO_2 neutrality.

More interesting is the consideration of the so-called ecological amortisation. This describes how long a turbine has to operate before it has generated the energy which is required to manufacture and operate it. The assumption for WTGs is 6 to 24 months [128] depending how high its capacity factor is. These values are so impressive because ecological amortisation for conventional power stations is not possible. They have to be continually fed with energy in the form of fuels, for example, to achieve an energy yield.

The design CO_2 footprint of a rotor blade is defined by the energy yield which it could theoretically produce under design conditions. WTGs and the rotor blade component in particular are often not subjected to the design loads during their planned lifetime so that the blades can continue to be operated either on the WTG at the site, or, if another component, e.g. the main shaft, limits the residual lifetime, on a different WTG at a site which may have lower wind speeds until the design loads are exploited, cf. [110]. The actual CO_2 footprint of a rotor blade is therefore usually larger than the design CO_2 footprint. Continued operation thus reduces the CO_2 footprint which then approaches the design CO_2 footprint. The unplanned removal and re-installation at a different site increases the CO_2 footprint again, however, because of the emissions from fossil fuels.

The question is therefore how WTGs can accomplish climate-neutral energy conversion particularly in respect of the rotor blade. This means in practice that the CO_2 footprint must be reduced in a first step and neutralised in a second.

The raw resources for the rotor blade materials are currently crude oil, sand, wood and to a lesser extent metals. To ideally reduce the CO_2 footprint of the materials to zero, this especially means not emitting the bound carbon compounds, which originate from the crude oil used as the basic resource, into the atmosphere by burning, for example, but keeping them in circulation.

This particularly concerns actions which take place after the end of the design life of the rotor blade. One option for neutralisation is to reuse structural elements of the blade, for example, in the form of support structures such as bridges. In the European Union, around 570 Mt of rotor blade waste is expected between 2020 and 2030 [118]. It is easy to imagine that, for various reasons, this amount cannot be used for bridges or other support structure alone.

An alternative is to deposit it in landfills, but this is already banned in some European countries. Although this does not release the carbon compounds of the fossil materials into the atmosphere, it does mean that the other valuable raw materials such as glass and wood are not returned to the cycle either. Several recycling methods are available to regenerate the bound raw materials as well as the bound energy.

One possibility is pyrolysis [17, 41], whereby the raw materials such as GF and CF as combustion residues can be reused in degraded form, i.e. as short fibres. The problem is that the crude-oil-based carbon compounds from the resin matrix are released in this process, because the matrix is burnt. Since the fibres cannot be reused in the same quality and with the same functionality as for the original material, this form of recycling corresponds to degraded recovery or downcycling.

With co-processing [119], the rotor blades are mechanically crushed and used as fuel for the production of cement, for example. Although this adds combustion residues from fossil materials to the atmosphere, the conventional fossil fuels used in cement manufacture are saved. The GF contained replaces sand fractions in the cement clinker. CF-reinforced EP composites are not suitable for cement co-processing. Co-processing is currently one of the few commercially available recycling options for rotor blade structures.

Further recycling options which are not yet commercially viable are mechanical grinding [136], solvolysis [75] and fragmentation by means of high-voltage pulse technology [80].

To reduce the CO_2 footprint further, organic-based raw materials can also be used as an alternative or in addition. EP resins which are produced partially on the basis of regenerative raw materials, for example, are already commercially available. Here the attempt is being made, among other things, to replace crude-oil-based raw materials such as bisphenol A (BPA). For the CF, 95 % of the total amount is currently manufactured on the basis of crude-oil-based polyacrylonitrile (PAN) precursors [35]. Research and development on alternatives for the crude-oil-based production of CF is currently underway as well [35]. Natural fibres such as flax, for example, initially have a smaller CO_2 footprint than CF or GF [6]. Since the mechanical properties of natural fibres are on the one hand worse and on the other subject to a larger statistical variability than industrially manufactured fibres, a higher mass of materials must accordingly be used in the blade to achieve the required stiffnesses and strengths. Whether this reduces the CO_2 footprint of the rotor blade must be answered on an individual basis. When the materials used are based completely on renewable raw materials, then even burning the components would be climate neutral.

Other options to meet the challenges of recycling can be preventative measures. For the current generation of rotor blades, use is sometimes already being made of

special EP curing agents which have been developed for a simplified solvolysis [29]. The residues can be admixed to thermoplastic matrix materials and used again in FRPs, while the fibre materials can be recovered. Whether these can be returned to a full use in structural materials is a research topic which is being investigated.

Furthermore, thermoplastic matrix materials can be used instead of polymer matrix materials. Pyrolysis is not necessary here because the composite can continue to be used, albeit it in lower quality applications of structural materials, since the structure is mechanically fragmented and converted into a thermally workable material. The advantage is that the carbon compounds in the matrix are not released. It goes without saying that this recycling option must already be planned during rotor blade development. Separating the thermoplastics matrix from the fibre materials simply by increasing the temperature is not possible without further ado since the viscosity of the matrix in the molten state is usually comparatively high.

At present, end-grain Balsa wood in particular is becoming scarce because of the globally increasing installed wind power [126]. The manufacturers are being forced to change to alternative core materials so as not to endanger supply chains. Alternative types of wood and also non-renewable raw materials based on conventional materials can be used as a fall-back here. The latter can even increase the CO_2 footprint of blades, when rotor blades are burnt or co-processed, for example. If recycled PET is used as the alternative, for example, it is removed from closed recycling loops, for example, for bottles [68] or in the textile industry for clothing, not simply for the service life of the rotor blade. The bonding with EP created in the manufacturing process, for example, means it can no longer be used in recycling, because the PET used can no longer be recycled in the same quality and fed into the recycling loops stated.

Finally, sustainable development also includes the fact that the natural regenerative ability of the systems involved (mainly living beings and ecosystems) is maintained [142]. In respect of the rotor blade, it should be mentioned that erosion can result in matrix and fibre materials getting into the ecosystem and thus into the food chain of organisms as well in the form of micro-particles or nano-particles. Especially when the EP matrix is based on BPA, ingesting the materials with food can be harmful to health [71].

This demonstrates that the materials used in rotor blades can currently not be recycled to a sufficient degree. Work is being done on promising approaches, however, to further improve the sustainability of the wind energy conversion. At this point it again becomes clear that the rotor blade must be considered and optimised in the context of the WTG system, and also in the context of the resource-efficient supply of energy for our society. As engineers, our task is to take up this challenge for the benefit of future generations. This is the only way that an energy supply based on equitable access to resources is possible for all humankind.

Literatures

1. Aero Dynamic Consult: ADCoS. https://www.aero-dynamik.de/Simulation_82.html
2. Ansys: Mechanical APDL. https://www.ansys.com/
3. Antoniou A, Rosemeier M, Tazefidan K, Krimmer A, Wolken-Möhlmann G (2020) Impact of site-specific thermal residual stress on the fatigue of wind-turbine blades. AIAA J 58(11):4781–4793. https://doi.org/10.2514/1.J059388
4. Basquin OH (1910) The exponential law of endurance tests. In: Proceedings of the thirteenth annual meeting, vol 10. American Society for Testing Materials, Atlantic City, New Jersey, USA, pp. 625–630. https://pdfcoffee.com/basquin-the-exponential-law-of-endurance-testspdf-pdf-free.html
5. Beelitz T, Hadzhiyski A, Kenfack R, Marzik J, Popiela B, Sahr R, Blümel T, Krimmer A (2021) Untersuchung des Torsionsverhaltens dünnwandiger, geschlossenzelliger Profilträger mit inhomogenem Querschnitt. In: Deutscher Luft- und Raumfahrtkongress 2021. Deutsche Gesellschaft für Luft- und Raumfahrt - Lilienthal-Oberth. https://doi.org/10.25967/550319
6. de Beus N, Carus M, Barth M (2019) Carbon footprint and sustainability of different natural fibres for biocomposites and insulation material. Tech. rep., Nova-Institute GmbH, Hürth, Germany. http://eiha.org/media/2019/03/19-03-13-Study-Natural-Fibre-Sustainability-Carbon-Footprint.pdf
7. Bir GS (2001) Computerized method for preliminary structural design of composite wind turbine blades. J Solar Energy Eng 123(4):372–381. https://doi.org/10.1115/1.1413217
8. Blasques JP, Stolpe M (2012) Multi-material topology optimization of laminated composite beam cross sections. Compos Struct 94(11):3278–3289. https://doi.org/10.1016/j.compstruct.2012.05.002
9. Bortolotti P, Bottasso CL, Croce A, Sartori L (2019) Integration of multiple passive load mitigation technologies by automated design optimization-the case study of a medium-size onshore wind turbine. Wind Energy 22(1):65–79. https://doi.org/10.1002/we.2270
10. Bosschers J (1996) Modelling of rotational effects with a 2-d viscous-inviscid interaction code. Tech. Rep. 96521. NLR—Netherlands Aerospace Centre, Amsterdam, the Netherlands
11. Bundeszentrale für politische Bildung: Auf Endlagersuche. Der deutsche Weg zu einem sicheren Atommülllager (2020). https://www.bpb.de/gesellschaft/umwelt/endlagersuche/315473/einleitung
12. Castro SGP, Rosemeier M (2019) Comput Mech (Compmech). https://github.com/mrosemeier/compmech
13. CEN: Eurocode: basis of structural design; EN 1990:2002 + A1:2005 + A1:2005/AC:2010. European Committee for Standardization (2010)
14. Cesnik CE, Hodges DH (1997) VABS: a new concept for composite rotor blade cross-sectional modeling. J Am Helicopter Soc 42(1):27–38. https://doi.org/10.4050/JAHS.42.27
15. Chen G, Wen J (2012) Load performance of large-scale rolling bearings with supporting structure in wind turbines. J Tribol 134(4):041105. https://doi.org/10.1115/1.4007349
16. Chou P, Carleone J, Hsu C (1972) Elastic constants of layered media. J Compos Mater 6(1):80–93. https://doi.org/10.1177/002199837200600107
17. Cunliffe A, Jones N, Williams P (2003) Pyrolysis of composite plastic waste. Environ Technol 24(5):653–663. https://doi.org/10.1080/09593330309385599
18. DAkkS: Datenbank der akkreditierten Stellen (2021). https://www.dakks.de/de/akkreditierte-stellen-suche.html
19. Danmarks Tekniske Universitet (DTU): Ellipsys. https://the-numerical-wind-tunnel.dtu.dk/EllipSys
20. Danmarks Tekniske Universitet (DTU): HAWC2. https://www.hawc2.dk
21. Dassault Systèmes: Simpack. https://www.3ds.com/products-services/simulia/products/simpack/product-modules/wind-modules/
22. Det Norske Veritas (DNV): Bladed. https://www.dnv.com/services/renewables-engineering-software-138662

23. DGfM: MauerWerk - Das Lehrportal - 3.1 Sicherheitskonzept. https://www.mauerwerksbau-lehre.de/vorlesungen/3-sicherheitskonzept-und-einwirkungen/31-sicherheitskonzept/311-allgemeine-grundlagen
24. DIBt: Richtlinie für Windenergieanlagen - Einwirkungen und Standsicherheitsnachweise für Turm und Gründung - Stand: Oktober 2012 - Korrigierte Fassung März 2015. Mitteilungen des DIBt, Technische Regel, Referat I 8, Bautechnisches Prüfamt, Grundlagen der Standsicherheit (2015). https://www.dibt.de/fileadmin/dibt-website/Dokumente/Referat/I8/Windenergieanlagen_Richtlinie_korrigiert.pdf
25. DNV: DNV-DS-J102 (2010) Design and manufacture of wind turbine blades, offshore and onshore wind turbines. https://rules.dnv.com/docs/pdf/dnvpm/codes/docs/2010-11/DS-J102.pdf
26. DNV GL: DNVGL-ST-0376 (2015) Rotor blades for wind turbines. https://www.dnv.com/energy/standards-guidelines/dnv-st-0376-rotor-blades-for-wind-turbines.html
27. DNV GL: DNVGL-SE-0441 (2016) Type and component certification of wind turbines. https://www.dnv.com/energy/standards-guidelines/dnv-se-0441-type-and-component-certification-of-wind-turbines.html
28. Drela M (1989) XFOIL: an analysis and design system for low Reynolds number airfoils. In: Mueller TJ (ed) Low Reynolds number aerodynamics. Springer, Berlin, Heidelberg, pp 1–12. https://doi.org/10.1007/978-3-642-84010-4_1
29. Dubey PK, Mahanth SK, Dixit A, Changmongkol S (2020) Recyclable epoxy systems for rotor blades. In: IOP conference series: materials science and engineering, vol 942. IOP Publishing. https://doi.org/10.1088/1757-899X/942/1/012014
30. ESI Group: Openfoam. https://www.openfoam.com/
31. Euler L (1744) Methodus inveniendi lineas curvas maximi minimive propietate gaudentes, Additamentum I, De curvis elasticis. Bousqet & Socios, Lausanne, Geneva, Switzerland. https://mdz-nbn-resolving.de/urn:nbn:de:bvb:12-bsb10053439-8
32. Feil R, Pflumm T, Bortolotti P, Morandini M (2020) A cross-sectional aeroelastic analysis and structural optimization tool for slender composite structures. Compos Struct 253:112755. https://doi.org/10.1016/j.compstruct.2020.112755
33. Fiedler B (2009) Hochleistungs-Faserverbundwerkstoffe mit Duroplastmatrix. Werkstoffe Struktur Eigenschaften Modellierung. TuTech Innovation GmbH, Hamburg, Germany
34. Fink R (2018) Einfluss der Materialkopplungen der klassischen Laminattheorie auf die Lage des Schubmittelpunktes mehrzelliger, dünnwandiger Profilquerschnitte. Technische Universität Berlin, Masterarbeit
35. Fraunhofer IAP (2019) Bio-based carbon fibers-high-performance and sustainability for light-weight applications. https://www.iap.fraunhofer.de/en/press_releases/2019/biobased-carbon-fibers.html
36. Fraunhofer IWES, MoWiT—Modelica for wind turbines library. https://www.iwes.fraunhofer.de/en/research-spectrum/entry-oem-supplier/aerodynamics-for-wind-turbines/Load-Calculations.html
37. Freymann R (2011) Strukturdynamik: Ein anwendungsorientiertes Lehrbuch. Springer, Berlin, Heidelberg, Germany (2011). https://doi.org/10.1007/978-3-642-19698-0
38. Galilei G (1638) Discorsi e dimostrazioni matematiche intorno à due nuoue scienze. Elsevier, Leiden, Netherlands. https://doi.org/10.3931/e-rara-3923
39. Gasch R, Knothe K, Liebich R (2012) Strukturdynamik: Diskrete Systeme und Kontinua, chap. 18–Bewegungsgleichungen von rotierenden elastischen Strukturen. Springer, Berlin, Heidelberg, Germany, pp 599–614. https://doi.org/10.1007/978-3-540-88977-9_18
40. Gere JM, Goodno BJ (2012) Mechanics of materials, 8th international edn. Nelson Education
41. Ginder RS, Ozcan S (2019) Recycling of commercial e-glass reinforced thermoset composites via two temperature step pyrolysis to improve recovered fiber tensile strength and failure strain. Recycl 4(2):24. https://doi.org/10.3390/recycling4020024
42. GL (2010) Guideline for the certification of wind turbines. Germanischer Lloyd Industrial Services, Hamburg, Germany

43. Goodman J (1899) Mechanics applied to engineering. Longmans, Green and Co., London, England. https://archive.org/details/mechanicsapplie03goodgoog
44. Griffith AA (1921) VI. The phenomena of rupture and flow in solids. Philos Trans R Soc London Ser A Contain Pap Math Phys Character 221(582–593):163–198. https://doi.org/10.1098/rsta.1921.0006
45. Habenicht G (2009) Kleben: Grundlagen, Technologie, Anwendungen, 6 edn. Springer, Berlin, Heidelberg, Germany. https://doi.org/10.1007/978-3-540-85266-7
46. Haibach E (2006) Betriebsfestigkeit, 3 edn. Springer, Berlin, Heidelberg, Germany. https://doi.org/10.1007/3-540-29364-7
47. Hansen MH (2007) Aeroelastic instability problems for wind turbines. Wind Energy 10(6):551–577. https://doi.org/10.1002/we.242
48. Hansen MOL (2015) Aerodynamics of wind turbines, 3rd edn. Routledge, London, UK
49. Hashin Z, Rosen B (1964) The elastic moduli of fiber-reinforced materials. J Appl Mech 31(2):223–232. https://doi.org/10.1115/1.3629590
50. Hauffe A (2020) Elamx^2. https://tu-dresden.de/ing/maschinenwesen/ilr/lft/elamx2/elamx
51. Heinz JC, Sørensen NN, Zahle F, Skrzypiński W (2016) Vortex-induced vibrations on a modern wind turbine blade. Wind Energy 19(11):2041–2051. https://doi.org/10.1002/we.1967
52. Hendriks H, Bulder B (1995) Fatigue equivalent load cycle method. A general method to compare the fatigue loading of different load spectrums. Tech. Rep. ECN-C-95-074. Energy research Centre of the Netherlands (ECN). https://www.ecn.nl/publicaties/PdfFetch.aspx?nr=ECN-C--95-074
53. Hodges DH (2006) Nonlinear composite beam theory. Am Inst Aeronaut Astronaut. https://doi.org/10.2514/4.866821
54. IEA (2019) Global energy & CO2 status report—The latest trends in energy and emissions in 2018. Tech. rep., Int Energy Agency. https://iea.blob.core.windows.net/assets/23f9eb39-7493-4722-aced-61433cbffe10/Global_Energy_and_CO2_Status_Report_2018.pdf
55. IEC (2010) IEC 61400-22—Wind turbines Part 22: conformity testing and certification. International Electrotechnical Commission, Geneva, Switzerland
56. IEC (2014) IEC 61400-23—Wind turbines Part 23: full-scale structural testing of rotor blades. International Electrotechnical Commission, Geneva, Switzerland
57. IEC (2018) IECRE OD-501—IEC system for certification to standards relating to equipment for use in renewable energy applications (IECRE System): type and component certification scheme. International Electrotechnical Commission, Geneva, Switzerland
58. IEC (2018) IECRE OD-501-1—IEC system for certification to standards relating to equipment for use in renewable energy applications (IECRE System): conformity assessment and certification of blade by RECB, 2 edn. International Electrotechnical Commission, Geneva, Switzerland
59. IEC (2019) IEC 61400-1—Wind energy generation systems—Part 1: design requirements, 4 edn. International Electrotechnical Commission, Geneva, Switzerland
60. IEC (2020) IEC 61400-5—Wind energy generation systems—Part 5: wind turbine blades. International Electrotechnical Commission, Geneva, Switzerland
61. IECRE (2021) RE testing laboratories (RETLs). https://test.iecre.org/dyn/www/f?p=110:7:::::P7_ORG_TYPE:RETL
62. Institut für Mechatronik in Chemnitz: alaska/Wind. https://www.ifm-chemnitz.de/produkte/alaskamultibodydynamics/alaskawind
63. ISO (1998) ISO 2394—General principles on reliability for structures. International Organization for Standardization, Geneva, Switzerland
64. ISO (2012) ISO/IEC 17065—Conformity assessment—Requirements for bodies certifying products, processes and services. International Organization for Standardization, Geneva, Switzerland
65. Jamieson P (2020) Top-level rotor optimisations based on actuator disc theory. Wind Energy Sci 5(2):807–818. https://doi.org/10.5194/wes-5-807-2020

66. Jonkman J, Musial W (2010) Offshore code comparison collaboration (oc3) for iea wind task 23 offshore wind technology and deployment. Tech. Rep. NREL/TP-5000-48191. National Renewable Energy Laboratory (NREL), Golden, Colorado, USA. https://doi.org/10.2172/1004009
67. Jørgensen JB, Sørensen BF, Kildegaard C (2018) The effect of buffer-layer on the steady-state energy release rate of a tunneling crack in a wind turbine blade joint. Compos Struct 188:64–71. https://doi.org/10.1016/j.compstruct.2017.12.081
68. K-ZEITUNG (2020) Das Branchenblatt der Kunststoffindustrie: Mit PET-Recycling zum geschlossenen Kunststoffkreislauf. https://www.k-zeitung.de/mit-pet-recycling-zum-geschlossenen-kunststoffkreislauf/
69. Kim T, Hansen AM, Branner K (2013) Development of an anisotropic beam finite element for composite wind turbine blades in multibody system. Renew Energy 59:172–183. https://doi.org/10.1016/j.renene.2013.03.033
70. Kollár LP, Springer GS (2003) Mechanics of composite structures. Cambridge University Press. https://doi.org/10.1017/CBO9780511547140
71. Konieczna A, Rutkowska A, Rachon D (2015) Health risk of exposure to Bisphenol A (BPA). Roczniki Państwowego Zakładu Higieny 66(1)
72. Krimmer A (2014) Mikromechanische Modellierung von Fasergelege-Kunststoff-Verbunden auf Basis von Normprüfungen unter Berücksichtigung der in-situ-Eigenschaften der Matrix. Ph.D. thesis, Technische Universität Berlin. https://doi.org/10.14279/depositonce-3869
73. Krimmer A (2017) Ermüdungsbewertung von Faser-Kunststoff-Verbunden am Beispiel von Rotorblättern. Lightweight Des 10(4):28–33. https://doi.org/10.1007/s35725-017-0037-0
74. Krimmer A, Leifheit R, Bardenhagen A (2016) Assessment of quasi-static and fatigue performance of uni-directionally fibre reinforced polymers on the basis of matrix effort. In: 6th EASN international conference on innovation in European aeronautics research. Porto, Portugal. https://doi.org/10.5281/zenodo.3878156
75. Kumar S, Krishnan S (2020) Recycling of carbon fiber with epoxy composites by chemical recycling for future perspective: a review. Chem Pap 74:3785–3807. https://doi.org/10.1007/s11696-020-01198-y
76. Lindenburg C, de Winkel G (2005) Buckling load prediction tools for rotor blades. Tech. Rep. ECN-C–05-103, Energy research Centre of the Netherlands ECN Wind Energy, Patten, the Netherlands. https://publicaties.ecn.nl/PdfFetch.aspx?nr=ECN-C--05-103
77. Madsen P, Dekker J, Thor S, McAnulty K, Matthies H, Thresher R (1990) Recommended practices for wind turbine testing, 3. fatigue loads, 2. edition. Tech. rep., International Energy Agency Programme for Research and Development on Wind Energy Conversion Systems
78. Mandell JF, Ashwill TD, Wilson TJ, Sears AT, Agastra P, Laird DL, Samborsky DD (2010) Analysis of SNL/MSU/DOE fatigue database trends for wind turbine blade materials. Tech. Rep. SAND2010-7052, Sandia National Laboratories, Albuquerque, New Mexico, USA. https://doi.org/10.2172/1034894
79. Mandell JF, Miller D, Samborsky D (2013) Creep/fatigue behavior of resin infused biaxial glass fabric laminates. In: 54th AIAA/ASME/ASCE/AHS/ASC structures, structural dynamics, and materials conference. American Institute of Aeronautics and Astronautics, Boston, Massachusetts, USA. https://doi.org/10.2514/6.2013-1630
80. Mativenga PT, Shuaib NA, Howarth J, Pestalozzi F, Woidasky J (2016) High voltage fragmentation and mechanical recycling of glass fibre thermoset composite. CIRP Annals 65(1):45–48. https://doi.org/10.1016/j.cirp.2016.04.107
81. Melcher D, Rosemann H, Haller B, Neßlinger S, Petersen E, Rosemeier M (2020) Proof of concept: elliptical biaxial rotor blade fatigue test with resonant excitation. In: IOP conference series: materials science and engineering, vol 942. IOP Publishing, p 012007. https://doi.org/10.1088/1757-899x/942/1/012007
82. Miner MA (1945) Cumulative damage in fatigue. J Appl Mech 12(3):A159–A164. https://doi.org/10.1115/1.4009458
83. Movahedi-Rad AV, Keller T, Vassilopoulos AP (2018) Fatigue damage in angle-ply GFRP laminates under tension-tension fatigue. Int J Fatigue 109:60–69. https://doi.org/10.1016/j.ijfatigue.2017.12.015

84. MSC Software: Adams/AdWiMo—Advanced wind turbine modeling. https://hexagon.com/support-success/manufacturing-intelligence/design-engineering-support/toolkit-solutions
85. Murray RE, Swan D, Snowberg D, Berry D, Beach R, Rooney S (2017) Manufacturing a 9 m thermoplastic composite wind turbine blade. In: 32nd technical conference on proceedings of the american society for composites (ASC). https://doi.org/10.12783/asc2017/15166
86. National Renewable Energy Laboratory (NREL) (2021) CCBlade. https://github.com/WISDEM/CCBlade
87. National Renewable Energy Laboratory (NREL) (2021) OpenFAST. https://github.com/OpenFAST/openfast
88. Nickel A (2011) Optimierung der Designparameter von GFK-Kern-Verbunden unter Berücksichtigung der Harzaufnahme des Kerns. Diplomarbeit, Technische Universität Berlin
89. Ning SA (2014) A simple solution method for the blade element momentum equations with guaranteed convergence. Wind Energy 17(9):1327–1345. https://doi.org/10.1002/we.1636
90. Øye S, Flex
91. Palmgren A (1924) Die Lebensdauer von Kugellagern. Zeitschrift des Vereins Deutscher Ingenieure 68(14):339–341
92. Pech A, Kolbitsch A, Zach F (2008) Tragwerke. Springer, Wien, Österreich. https://doi.org/10.1007/978-3-211-33032-6
93. Peeters M, Santo G, Degroote J, Van Paepegem W (2018) Comparison of shell and solid finite element models for the static certification tests of a 43 m wind turbine blade. Energies 11(6):1346. https://doi.org/10.3390/en11061346
94. Peeters M, Santo G, Degroote J, Van Paepegem W (2018) High-fidelity finite element models of composite wind turbine blades with shell and solid elements. Compos Struct 200:521–531. https://doi.org/10.1016/j.compstruct.2018.05.091
95. Politecnico di Milano: Cp-Lambda. http://www.poliwind.polimi.it/
96. Popko W, Huhn ML, Robertson A, Jonkman J, Wendt F, Müller K, Kretschmer M, Vorpahl F, Hagen TR, Galinos C, Le Dreff JB, Gilbert P, Auriac B, Víllora FN, Schünemann P, Bayati I, Belloli M, Oh S, Totsuka Y, Qvist J, Bachynski E, Sørum SH, Thomassen PE, Shin H, Vittori F, Galván J, Molins C, Bonnet P, van der Zee T, Bergua R, Wang K, Fu P, Cai J (2018) Verification of a numerical model of the offshore wind turbine from the alpha ventus wind farm within OC5 phase III. In: 37th international conference on ocean, offshore and arctic engineering. American Society of Mechanical Engineers. https://doi.org/10.1115/OMAE2018-77589
97. Previtali F, Eyb E (2021) An improved approach for the fatigue calculation of rotor blades based on sector loads. Wind Eng. https://doi.org/10.1177/0309524X20985320
98. Puck A (1996) Festigkeitsanalyse von Faser-Matrix-Laminaten: Modelle für die Praxis. Hanser, Munich, Germany
99. Quaschning V (2021) Erneuerbare Energien und Klimaschutz: Hintergründe–Techniken und Planung–Ökonomie und Ökologie–Energiewende, 6 edn. Hanser, Munich, Germany. https://doi.org/10.3139/9783446468689
100. Rahmstorf S (2019) Wie viel CO2 kann Deutschland noch ausstoßen? https://scilogs.spektrum.de/klimalounge/wie-viel-co2-kann-Deutschland-noch-ausstossen/
101. Reddy JN (2003) Mechanics of laminated composite plates and shells: theory and analysis, 2 edn. CRC Press, Boca Raton, Florida, USA. https://doi.org/10.1201/b12409
102. Rinker J, Gaertner E, Zahle F, Skrzypiński W, Abbas N, Bredmose H, Barter G, Dykes K (2020) Comparison of loads from HAWC2 and OpenFAST for the IEA Wind 15 MW reference wind turbine. J Phys: Conf Ser 1618:052052. IOP Publishing. https://doi.org/10.1088/1742-6596/1618/5/052052
103. Rosemeier M (2013) Non-linear ultimate limit state analysis of a wind turbine blade. Master's thesis, Hochschule Bremerhaven, Munich, Germany. https://www.grin.com/document/211296
104. Rosemeier M, Antoniou A (2021) Probabilistic approach for the fatigue strength prediction of polymers. AIAA J 60(2):951–961. https://doi.org/10.2514/1.J060444
105. Rosemeier M, Bätge M (2014) A concept study of a carbon spar cap design for a 80m wind turbine blade. J Phys: Conf Ser 524:012039 (IOP Publishing). https://doi.org/10.1088/1742-6596/524/1/012039

106. Rosemeier M, Berring P, Branner K (2016) Non-linear ultimate strength and stability limit state analysis of a wind turbine blade. Wind Energy 19(5):825–846. https://doi.org/10.1002/we.1868
107. Rosemeier M, Buriticá P, Antoniou A (2018) Impact of resin uptake of core materials on buckling of wind turbine blades. J Phys: Conf Ser 1037:042001 (IOP Publishing). https://doi.org/10.1088/1742-6596/1037/4/042001
108. Rosemeier M, Krimmer A, Antoniou A (2020) Development of thermal residual stresses during manufacture of wind turbine blades. J Phys: Conf Ser 1452:012060 (IOP Publishing). https://doi.org/10.1088/1742-6596/1452/1/012060
109. Rosemeier M, Krimmer A, Bardenhagen A, Antoniou A (2019) Tunneling crack initiation in trailing-edge bond lines of wind-turbine blades. AIAA J 57(12):5462–5474. https://doi.org/10.2514/1.J058179
110. Rosemeier M, Saathoff M (2020) Assessment of a rotor blade extension retrofit as a supplement to the lifetime extension of wind turbines. Wind Energy Sci 5(3):897–909. https://doi.org/10.5194/wes-5-897-2020
111. Rosemeier M, Saathoff M (2020) Impact of manufacture-induced blade shape distortion on turbine loads and energy yield. https://doi.org/10.5281/zenodo.4058566
112. Saathoff M, Rosemeier M, Kleinselbeck T, Rathmann B (2021) Effect of individual blade pitch angle misalignment on the remaining useful life of wind turbines. Wind Energy Sci 6(5):1079–1087. https://doi.org/10.5194/wes-6-1079-2021
113. Schleich F, Stammler M (2019) Realitätsgetreue Abbildung von Rotorblattlagerbelastungen durch Berücksichtigung der Anschlusssteifigkeiten. In: VDI-Berichte 234813. VDI-Fachtagung Gleit- und Wälzlagerungen 2019. Gestaltung - Berechnung - Einsatz: Schweinfurt, vol 2348. Verein Deutscher Ingenieure, pp 209–220. https://doi.org/10.51202/9783181023488-209
114. Schlömer S, Bruckner T, Fulton L, Hertwich E, McKinnon A, Perczyk D, Roy J, Schaeffer R, Sims R, Smith P, Wiser R (2014) 2014: Annex III: technology-specific cost and performance parameters. In: Edenhofer O, Pichs-Madruga R, Sokona Y, Farahani E, Kadner S, Seyboth K, Adler A, Baum I, Brunner S, Eickemeier P, Kriemann B, Savolainen J, Schlömer S, von Stechow C, Zwickel T, Minx JC (eds) Climate change 2014: mitigation of climate change. Contribution of working group III to the fifth assessment report of the intergovernmental panel on climate change. Cambridge University Press. https://www.ipcc.ch/site/assets/uploads/2018/02/ipcc_wg3_ar5_annex-iii.pdf
115. Schümann JP (2019) Zur zeit-, temperatur- und umsatzabhängigen Entwicklung polymerphysikalischer Vernetzungsschwindung aminisch vernetzender Epoxide. Ph.D. thesis, Technische Universität Clausthal, Clausthal, Germany. https://doi.org/10.21268/20190306-0
116. Schürmann H (2007) Konstruieren mit Faser-Kunststoff-Verbunden, 2 edn. Springer. https://doi.org/10.1007/978-3-540-72190-1
117. Skjoldan PF (2011) Aeroelastic modal dynamics of wind turbines including anisotropic effects. Ph.D. thesis, Danmarks Tekniske Universitet, Risø Nationallaboratoriet for Bæredygtig Energi. https://backend.orbit.dtu.dk/ws/portalfiles/portal/5509069/ris-phd-66.pdf
118. Sommer V, Stockschläder J, Walther G (2020) Estimation of glass and carbon fiber reinforced plastic waste from end-of-life rotor blades of wind power plants within the European union. Waste Manag 115:83–94. https://doi.org/10.1016/j.wasman.2020.06.043
119. Sommer V, Walther G (2021) Recycling and recovery infrastructures for glass and carbon fiber reinforced plastic waste from wind energy industry: a European case study. Waste Manag 121:265–275. https://doi.org/10.1016/j.wasman.2020.12.021
120. Stiesdal H, Enevoldsen PB, Johansen K, Kristensen JJ, Noertem M, Winther-Jensen M (2001) Verfahren zur Herstellung von Windmühlenflügeln. https://worldwide.espacenet.com/patent/search/family/026069092/publication/DE60210729T2?q=pn%3DDE60210729T
121. Suresh S (2003) Fatigue of materials, 2 edn. Cambridge University Press, Cambridge, UK. https://doi.org/10.1017/CBO9780511806575

122. Sutherland H, Mandell J (2005) Optimized goodman diagram for the analysis of fiberglass composites used in wind turbine blades. In: 43rd AIAA aerospace sciences meeting and exhibit. American Institute of Aeronautics and Astronautics. https://doi.org/10.2514/6.2005-196
123. Tareq MS, Jony B, Zainuddin S, Al Ahsan M, Hosur MV (2021) Fatigue analysis and fracture toughness of graphene reinforced carbon fibre polymer composites. Fatigue Fract Eng Mater Struct 44(2):461–474. https://doi.org/10.1111/ffe.13371
124. Technische Universität Berlin - Institut für Strömungsmechanik und Technische Akustik - Fachgebiet Experimentelle Strömungsmechanik: Qblade (2016). http://www.q-blade.org
125. Technische Universität Darmstadt - Fachgebiet Konstruktiver Leichtbau und Bauweisen (KLuB): Alfalam (2009)
126. The Economist—The Americas: a worrying windfall—The wind-power boom set off a scramble for balsa wood in Ecuador (2020). https://www.economist.com/the-americas/2021/01/30/the-wind-power-boom-set-off-a-scramble-for-balsa-wood-in-ecuador
127. Thomason JL (2019) Glass fibre sizing: a review. Compos Part A: Appl Sci Manuf 127:105619. https://doi.org/10.1016/j.compositesa.2019.105619
128. Thomson C, Harrison G (2015) Life cycle costs and carbon emissions of wind power: executive summary. Tech. rep., University of Edinburgh, Edinburgh, Scotland. https://www.climatexchange.org.uk/media/1459/life_cycle_wind_-_executive_summary_.pdf
129. Timoshenko SP (1921) LXVI. On the correction for shear of the differential equation for transverse vibrations of prismatic bars. London Edinburgh Dublin Philos Mag J Sci 41(245):744–746. https://doi.org/10.1080/14786442108636264
130. TPI Composites (2019) TPI composites blade manufacturing process. https://youtu.be/jpRudTUIyfM
131. UNO (1987) Report of the world commission on environment and development: our common future. Organisation der Vereinten Nationen. https://www.are.admin.ch/dam/are/de/dokumente/nachhaltige_entwicklung/dokumente/bericht/our_common_futurebrundtlandreport1987.pdf.download.pdf
132. UNO (2015) TREATIES-XXVII.7.d Paris agreement. Organisation der Vereinten Nationen. https://treaties.un.org/doc/Treaties/2016/02/20160215%2006-03%20PM/Ch_XXVII-7-d.pdf
133. Varik MV (2013) FINSTRIP: theoretical reference. Knowledge Centre WMC
134. VDI (2003) VDI 2230 Part 1—Systematic calculation of high duty bolted joints Joints with one cylindrical bolt. Verein Deutscher Ingenieure, Düsseldorf, Germany
135. VDI (2006) VDI 2014 Part 3 development of FRP components (fibre-reinforced plastics) analysis. Verein Deutscher Ingenieure, Düsseldorf, Germany
136. Vincent GA, de Bruijn TA, Wijskamp S, Rasheed MIA, van Drongelen M, Akkerman R (2019) Shredding and sieving thermoplastic composite scrap: method development and analyses of the fibre length distributions. Compos Part B: Eng 176:107197. https://doi.org/10.1016/j.compositesb.2019.107197
137. Wang Q, Sprague MA, Jonkman JM (2014) Nonlinear Legendre spectral finite elements for wind turbine blade dynamics. In: 32nd ASME wind energy symposium, p. 1224. American Institute of Aeronautics and Astronautics, National Harbor, Maryland, USA. https://doi.org/10.2514/6.2014-1224
138. Wang Q, Sprague MA, Jonkman JM (2016) Partitioned nonlinear structural analysis of wind turbines using Beamdyn. In: 34th wind energy symposium. American Institute of Aeronautics and Astronautics, San Diego, Kalifornien, USA, p 0753. https://doi.org/10.2514/6.2016-0753
139. Wang Q, Yu W (2017) Geometrically nonlinear analysis of composite beams using wiener-milenković parameters. J Renew Sustain Energy 9(3):033306. https://doi.org/10.1063/1.4985091
140. Wang S, Zhang C (2014) Structure mechanical modeling of thin-walled closed-section composite beams, part 2: multi-cell cross section. Compos Struct 113:56–62. https://doi.org/10.1016/j.compstruct.2014.03.002

141. Wiedemann J (2007) Leichtbau: Elemente und Konstruktion, 3 edn. Springer, Berlin, Heidelberg, New York. https://doi.org/10.1007/978-3-540-33657-0
142. Wikipedia (2021) Die freie Enzyklopädie: Nachhaltigkeit. https://de.wikipedia.org/wiki/Nachhaltigkeit
143. Wittel H, Jannasch D, Voßiek J, Spura C (2019) Roloff/Matek Maschinenelemente, 24 edn. Springer Viewer. https://doi.org/10.1007/978-3-658-26280-8
144. Wlassow WS (1959) Dünnwandige elastische Stäbe, vol 1, 2 edn. Staatsverlag für physikalisch-mathematische Literatur, Moscow, Soviet Union
145. WMC Technology Center Netherlands: FOCUS6
146. Zangenberg J, Brøndsted P, Gillespie Jr JW (2014) Fatigue damage propagation in unidirectional glass fibre reinforced composites made of a non-crimp fabric. J Compos Mater 48(22):2711–2727. https://doi.org/10.1177/0021998313502062
147. Zhang C, Wang S (2014) Structure mechanical modeling of thin-walled closed-section composite beams, part 1: single-cell cross section. Compos Struct 113:12–22. https://doi.org/10.1016/j.compstruct.2014.03.005

M.Sc. Malo Rosemeier has been working as a research assistant at the Fraunhofer Institute for Wind Energy Systems IWES since 2013. In the Rotor Blades department, he is responsible for applied research on blade structures. The focus is on the development of validation tests and structural analysis methods, among other things.

Dr. Alexander Krimmer works as Senior Engineer Composite Materials and Structures at TPI Composites Germany GmbH. There he is responsible for qualification, specification, evaluation and preparation for certification of structural materials for wind turbine rotor blades. In addition, he teaches at the Department of Aircraft Construction and Lightweight Design at the Institute of Aeronautics and Astronautics at the TU Berlin in the modules of fibre composite lightweight construction as well as production and design of fibre-reinforced plastic composites.